

DECEMBER 1965

LMSC-667990

# FORCES INDUCED ON BODIES IN FREE WAKES AND THREE-DIMENSIONAL CAVITIES

N 66 26231

FACILITY FORM 602

(ACCESSION NUMBER)	(THRU)
86	1
(PAGES)	(CODE)
100	01
(NASA CR OR TMX OR AD NUMBER)	(CATEGORY)

# Lockheed

## MISSILES & SPACE COMPANY

A GROUP DIVISION OF LOCKHEED AIRCRAFT CORPORATION  
SUNNYVALE, CALIFORNIA

GPO PRICE \$ \_\_\_\_\_

CFSTI PRICE(S) \$ \_\_\_\_\_

Hard copy (HC) # 2.00

Microfiche (MF) 1.50

CLASSIFIED

LOCKHEED MISSILES AND SPACE COMPANY  
A Division of Lockheed Aircraft Corporation


Technical Memorandum

LMSC/667990

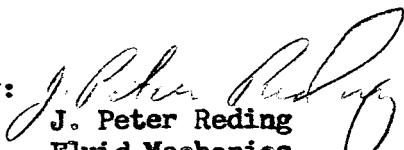
FORCES INDUCED ON  
BODIES IN FREE WAKES AND  
THREE-DIMENSIONAL CAVITIES

DECEMBER 1965


Checked By:

  
Lars-Eric Ericsson  
Staff Engineer, Sr.  
Flight Technology

Prepared By:

  
J. Peter Reding  
Fluid Mechanics  
Aero-Hydrodynamics

Approved By:

  
M. Tucker  
Manager  
Flight Technology

Prepared Under Contract NAS 8-5338  
for  
Aerodynamics Division, Aero-Astrodynamic Laboratory  
George C. Marshall Space Flight Center  
National Aeronautics and Space Administration  
Huntsville, Alabama

ABSTRACT

26231

Deformed wind tunnel models have been used in an experimental investigation of the loads on bodies in wakes, thus allowing the measurement of both local and wake source dependent submerged body loads. An analysis of these data reveal that the application of the separated to attached flow axial force ratio to the computation of the local Apollo command module load is valid. However, as the wake source to submerged body distance is increased a critical range is experienced where large induced upstream communication effects occur. These upstream effects amplify the loads dependent upon wake source conditions as well as those that result from the local submerged body crossflow, and could, therefore, seriously alter the vehicle dynamics.

TABLE OF CONTENTS

	<u>Page</u>
ABSTRACT	iii
ILLUSTRATIONS	vii
SUMMARY	1
INTRODUCTION	3
FORCE DATA REDUCTION	5
RESULTS AND DISCUSSION	11
WAKE VELOCITY DEFICIT	12
UPSTREAM COMMUNICATION EFFECTS	13
AFT CYLINDER LOADS	35
CONCLUSIONS	47
REFERENCES	49
APPENDIX	
A NOMENCLATURE	A-1
B FINAL CORRECTIONS TO THE FORCE DERIVATIVES	B-1

ILLUSTRATIONS

<u>Figure</u>		<u>Page</u>
1	Schematic Illustration of Variables	7
2	Sample Carpet Plot	9
3	Submerged Body Axial Force for Various Wake Sources ( $\alpha = 0$ )	14
4	Correlation of Submerged Body Axial Force Ratio with Wake Source Axial Force ( $M = .9$ )	16
5	Local Crossflow Effects on the Submerged Conic Forebody (Directing Wake Source)	17
6	Effect of Submerged Body on Maximum Wake Source Base Pressure (Elliptic Wake Source)	20
7	Correlation of Wake Source Base Pressure Sensitivity with Submerged Conic Forebody Local Loads	21
8	Wake Translation Effects on the Submerged Conic Forebody	28
9	Comparison of Wake Directing Effects on the Submerged Conic Forebody	30
10	Effect of Wake Mach Number Gradient	32
11	Effect of Submerged Body Proximity on Wake Source Axial Force (Elliptic Wake Source)	34
12	Effect of Submerged Body Proximity on Wake Source Normal Force Derivative (Elliptic Wake Source)	36
13	Aft Cylinder Local Loads	38
14	Aft Cylinder Local Crossflow Center of Pressure	39
15	Submerged Conic Forebody Local Crossflow Center of Pressure	40
16	Wake Translation Effects on Aft Cylinder Loads	41
17	Wake Translation Effects on Aft Cylinder Center of Pressure	42

ILLUSTRATIONS (Cont'd)

<u>Figure</u>		<u>Page</u>
18	Wake Translation Effects on the Submerged Conic Forebody Center of Pressure	44
19	Wake Directing Effects on the Aft Cylinder Loads	45
20	Wake Directing Effects on the Aft Cylinder Center of Pressure	45
21	Wake Directing Effects on the Conic Forebody Center of Pressure	46

SUMMARY

The loads generated on a body submerged in a wake are dependent upon the geometry, attitude, and relative displacement of the wake generating forebody as well as the submerged body geometry and attitude. This aerodynamic coupling between the wake source and the submerged body has a large influence on the vehicle dynamics, and a complete understanding of coupling effects is needed to predict the vehicle dynamics. To facilitate such an understanding an investigation of the static loads produced on a submerged body has been accomplished. Using deformed models and automated carpet plot techniques the static loads caused by each mode of wake source and submerged body motion have been obtained. The results substantiate the veracity of the simple assumptions made in the dynamic analysis of the Saturn vehicles. For greater wake source distances upstream communications effects occur which are larger than the more conventional wake induced loads and thus may have a large dynamic effect.

INTRODUCTION

The loads induced by the escape rocket wake on the Saturn-Apollo vehicles constitute the greatest single separated flow loading on these vehicles (Ref. 1 and 2). The aerodynamic damping of these vehicles, as influenced by flow separation, was computed from static experimental data (Ref. 1). In order to make these computations the static data were subject to some interpretation to determine the fractional dependence of the measured total load on the various modes of wake source and submerged body motion. The following basic propositions were fundamental to the quasi-steady technique:

- 1) That the wake source induces loads on a body submerged in its wake by virtue of both its attitude and displacement relative to the submerged body;
- 2) That the load generated by crossflow over a body submerged in a wake is less than for the same body in attached flow due to the reduced wake dynamic pressure;
- 3) That the reduced wake dynamic pressure may be related to the reduced submerged body axial force.

To verify these propositions a wind tunnel program was carried out wherein various models with tower mounted wake sources were tested. On each model the tower was deformed such that either wake source pitch or relative displacement was simulated. These deformed models were pitched and the resulting force data were carpet plotted to obtain the cross derivatives simulated by tower deformation. The reduction of the data (including corrections for



tower deflection under load, manufacturing tolerances, wake source to balance misalignments, and automatic plotting of the reduced data) involved a considerable programming effort which is discussed fully in Ref. 3. In what follows the testing technique and carpet plotting procedure will be discussed briefly for background before presenting the results of the analysis.

FORCE DATA REDUCTION

In the analysis of the Saturn vehicles it was postulated that three separate normal force derivatives acted on a body submerged in a wake (Ref. 1). The first was the usual local attitude dependent derivative  $C_{N\alpha_s}$  (where  $s$  denotes that the body is submerged in separated flow). The remaining two derivatives,  $\Delta^i C_{N_z}$  and  $\Delta^i C_{N_\theta}$ , are functions of conditions at the wake source and are termed "induced" derivatives. Both result from translating the wake over the submerged body. Referring to the shadowgraph of Fig. 1 one may see that the wake is translated to the leeward side of the submerged body by virtue of the relative position of the two bodies. However, because the wake source is slender the wake is directed initially downward at the wake source for positive wake source attitudes thus reducing the amount of translation due to relative displacement, i.e., causing a negative translation. The two induced derivatives may be defined, with the help of Fig. 1, as follows:

$\Delta^i C_{N_z}$  is the relative displacement or translating derivative.

$\Delta^i C_{N_\theta}$  is the wake source attitude dependent derivatives.

For small displacements one may express the translating derivative as

$$\Delta^i C_{N_z} = \frac{1}{\ell} \Delta^i C_{N_\beta}$$

where  $\ell$  is the distance between the wake source and the normal force vector.

It was these three derivatives that were measured in this test program along with their associated moments and axial forces. Due to practical manufacturing

constraints the various derivatives were not necessarily measured directly. For instance, separate models were made with the tower and wake source pitched relative to the submerged body. Thus, the wake source attitude was not zero for these cases but was nominally equal to the tower attitude. Furthermore, the tower attitude,  $\delta_t$ , was not equal to  $\beta$ . However, the two are related as defined below with the help of Fig. 1.

$$\beta \approx \tan \beta = \frac{z}{l}$$

$$\delta_t \approx \tan \delta_t = \frac{z}{x}$$

therefore,  $\beta l = \delta_t x$

thus  $\frac{\delta_t}{\beta} = \frac{l}{x}$

The wake source attitude was varied directly and its effects could then be subtracted from the uncorrected translatory derivative ( $\beta_u$ ) to obtain the  $\beta$  derivative.

It was necessary to make separate models for each wake source or tower deflection. Therefore, the procedure followed was to obtain coefficient versus  $\alpha$  results and to carpet plot to obtain the forebody dependent slopes. The data reduction procedure was further complicated by the effects of manufacturing tolerances, as it was impossible to hold  $\delta_t = 0$  for  $\theta_t$  - variations or to have  $\theta_t = 0$  for  $\delta_t$  - variations. Furthermore, the tower was not completely rigid and under-went deflections under load that had to be accounted for. It was, therefore, necessary to carpet plot the data using the nominal values of  $\theta_t$  and  $\delta_t$ . The data were then curve fitted and corrections were made for the misalignments.

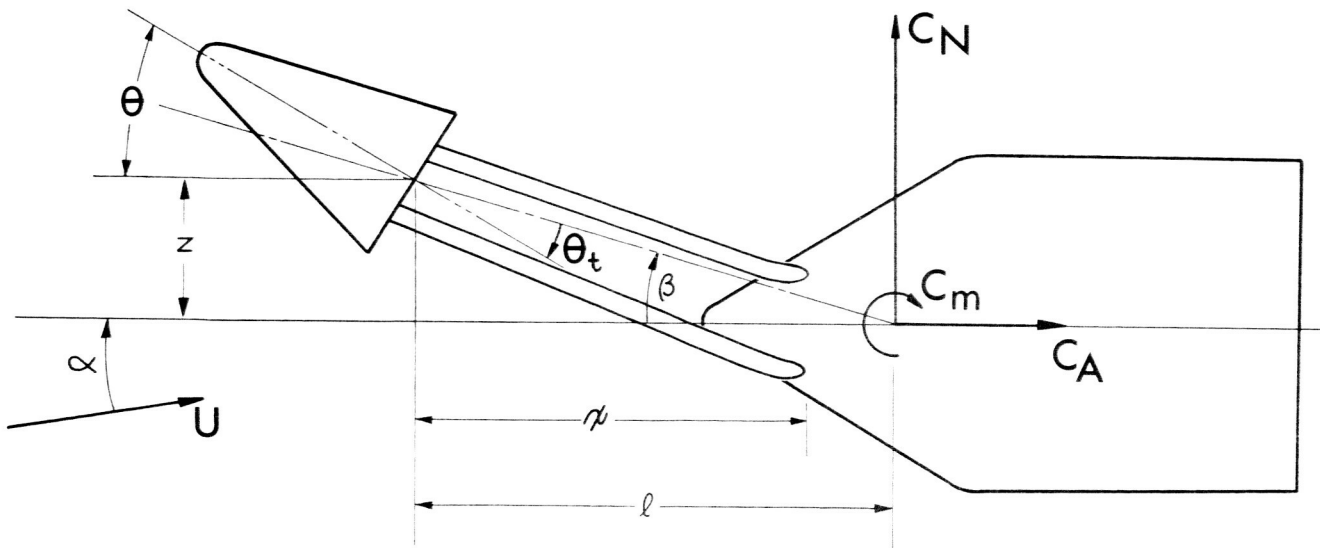
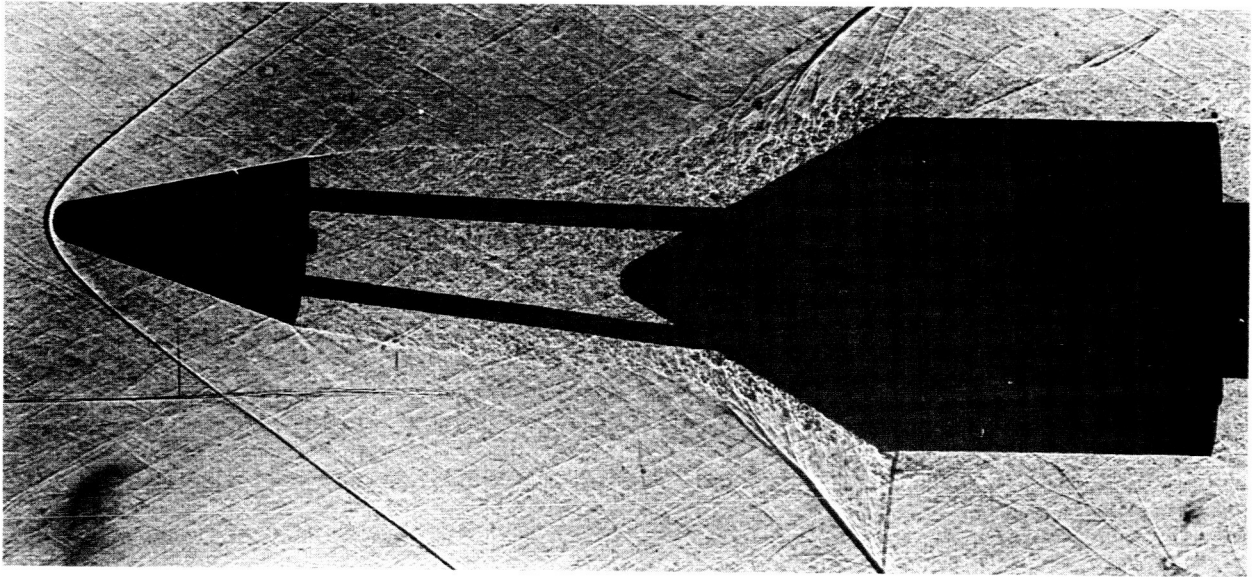


Fig. 1 Schematic Illustration of Variables

This process was repeated until the magnitude of the correction was within acceptable limits (Ref. 3). The  $\delta_t$  derivatives were then transformed to  $\beta_u$  derivatives (including  $\theta$  loads). A sample corrected, transformed, carpet plot is shown in Figure 2. Finally slopes of the carpet plotted data were corrected for wake source loads and the effects of  $\theta$  were eliminated from the  $\beta_u$  derivatives. These final corrections are outlined in Appendix B. The final data output was then the angle of attack derivatives, the  $\theta$  and  $\beta$  induced derivatives, and the separately measured wake source loads. The submerged body loads are related as follows:

$$C_{N_s} = \Delta^i C_{N_\theta} + \Delta^i C_{N_\beta} + C_{N_s} \quad (1)$$

Thus, although they were not measured directly, the three force derivatives which make up the submerged body load were obtained from the data.

NORMAL FORCE VERSUS ANGLE OF ATTACK

U1107/SC4020  
0000 0015

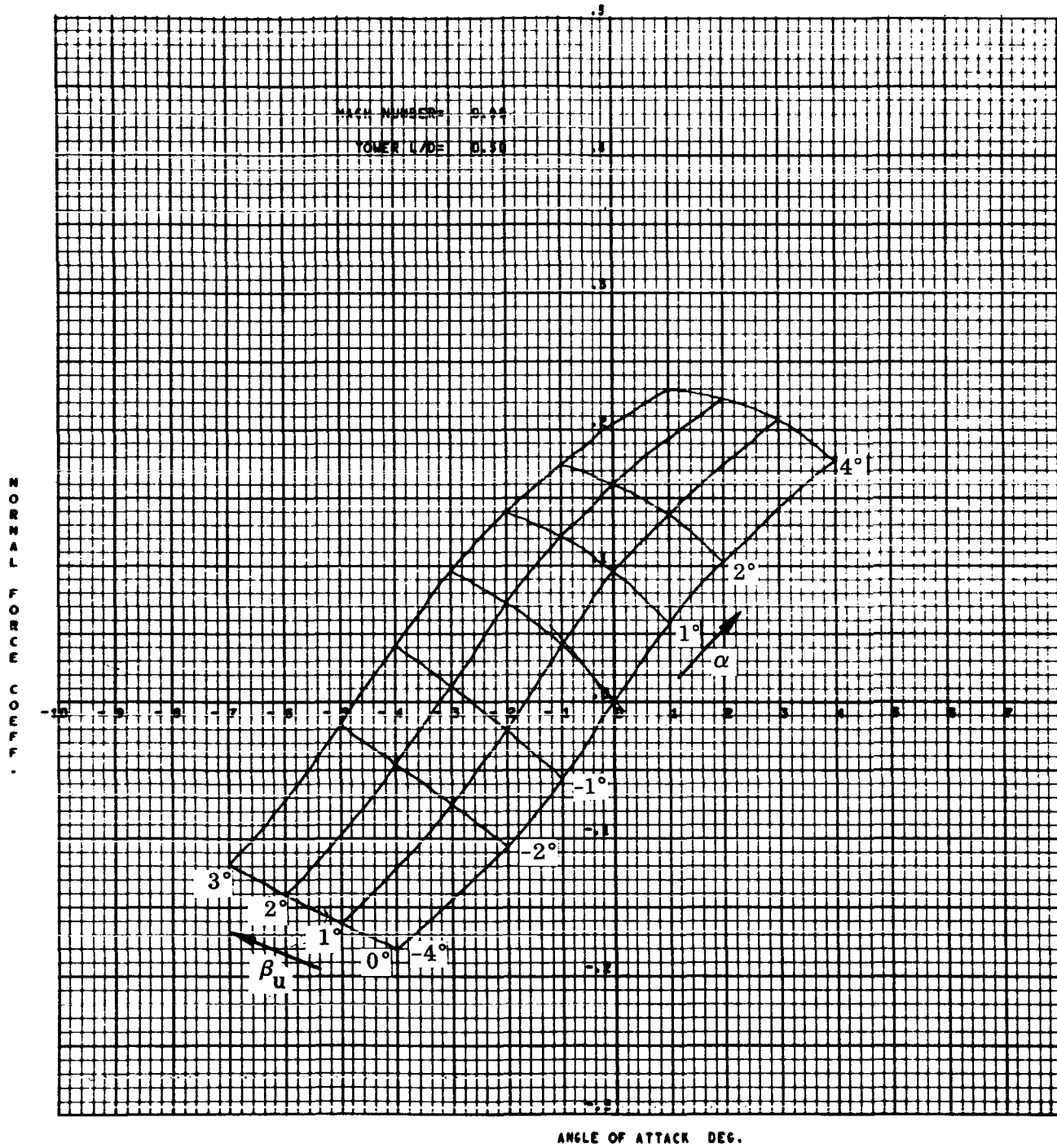


Fig. 2 Sample Carpet Plot

RESULTS AND DISCUSSION

The ability to calculate the aerodynamic damping in regions of separated flow hinges on being able to split the loads on the submerged body into the components dependent on local crossflow and those dependent upon conditions at the separation source. Since the axial force of a body submerged in separated flow is less than for attached flow, it was suggested in Ref. 1 that the reduced axial force could be used as a measure of the dynamic pressure in the wake.

$$\text{Thus, } \frac{q_s}{q_{\infty}} = \frac{(C_{A_0})_s}{(C_{A_0})_a} \quad (2)$$

where a refers to attached flow and s to separated flow. Furthermore, the normal forced derivative produced by pitching a body within the reduced dynamic pressure field of a wake was assumed to be simply

$$C_{N_{\alpha s}} = C_{N_{\alpha a}} \frac{(C_{A_0})_s}{(C_{A_0})_a} \quad (3)$$

The induced load may then be found from the total submerged body normal force derivative

$$\Delta^i C_{N_{\alpha}} = C_{N_{\alpha}} - C_{N_{\alpha s}} \quad (4)$$

where

$$\Delta^i C_{N_{\alpha}} = \Delta^i C_{N_{\beta}} + \Delta^i C_{N_{\theta}} \quad (5)$$

The data obtained in this test program (published in Ref. 4 and 5) tests the veracity of these assumptions.

Wake Velocity Deficit

That there is a reduction in the axial force is amply demonstrated in Fig. 3 (and Ref. 6 through 8 as well). As the wake source distance (distance between wake source and submerged body) is increased the submerged body axial force approaches the attached flow value. This results from the wake closing forward of the submerged body (cutting off the low velocity recirculating wake core) and the viscous interaction with the free stream flow increasing the wake velocity. The trends in Fig. 3 also indicate that for higher drag wake sources the submerged body axial force decreases. As a matter of fact the disk wake source causes the submerged body axial force to go negative at  $M = .9$  for wake source distance less than about 1.9 submerged body calibers. This "three dimensional cavity" effect results from reattachment occurring well aft of the conic portion of the submerged body. Roshko (Ref. 9) has measured negative static pressures on the downstream face of a cavity at subsonic speeds and Nicoll (Ref. 10) has presented data for "step-down" cavities on a conic surface that show decreasing cavity pressure for hypersonic Mach numbers as the step height increases. An extrapolation of Nicoll's data indicates the existence of negative cavity pressures. Evidently the flow attaching aft of the cavity (on the cylindrical portion of the submerged body in this case) has a low reverse mass flow rate and there is a tendency to aspirate the cavity. The minimum pressures obtainable in the cavity would of course be the wake source base pressure which the submerged body axial force seems to be approaching as the wake source distance goes to zero. Examination of the shadowgraphs of Figure 3 indicate that reattachment occurs aft of the conic surface for all



configurations; however, no discernible reattachment occurs for the disk wake source indicating very little reverse flow\* and substantiating the aspirating effect.

The trend of reduced submerged body axial force with increasing wake source axial force shown in Fig. 3 suggests the existence of some correlation between the two. The wake source axial force is a direct measurement of the wake momentum deficit and could be used to predict the submerged body axial force if reattachment occurred on the cone. Unfortunately, reattachment occurred well aft of the cone for the configurations tested; however, it appears that one could establish some empirical correlation between the submerged body axial force ratio and the wake source axial force (Fig. 4).

#### Upstream Communication Effects

One of the primary purposes of this test program was to verify the use of the axial force ratio in splitting the submerged body load into local and induced components. Examination of the loads on the  $30^\circ$  conical portion of the submerged body indicate a deviation from the results computed using the axial force ratio (Eq. 3). Good agreement occurs for a .5 caliber wake source distance but then the curves deviate (Fig. 5) with the experimental data showing a  $C_{N_x}$  as much as 6 or 7 times above that predicted from the axial force ratio at a wake source distance of approximately 1.0 caliber. The curves converge again for larger wake source distances as attached flow conditions are approached

---

\* Some of the wake flow must be turned back. However, judging by the extent of the wake it must indeed be only the low velocity core.

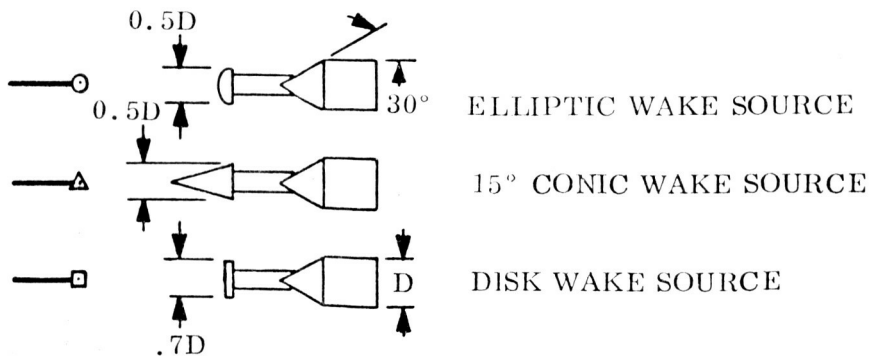
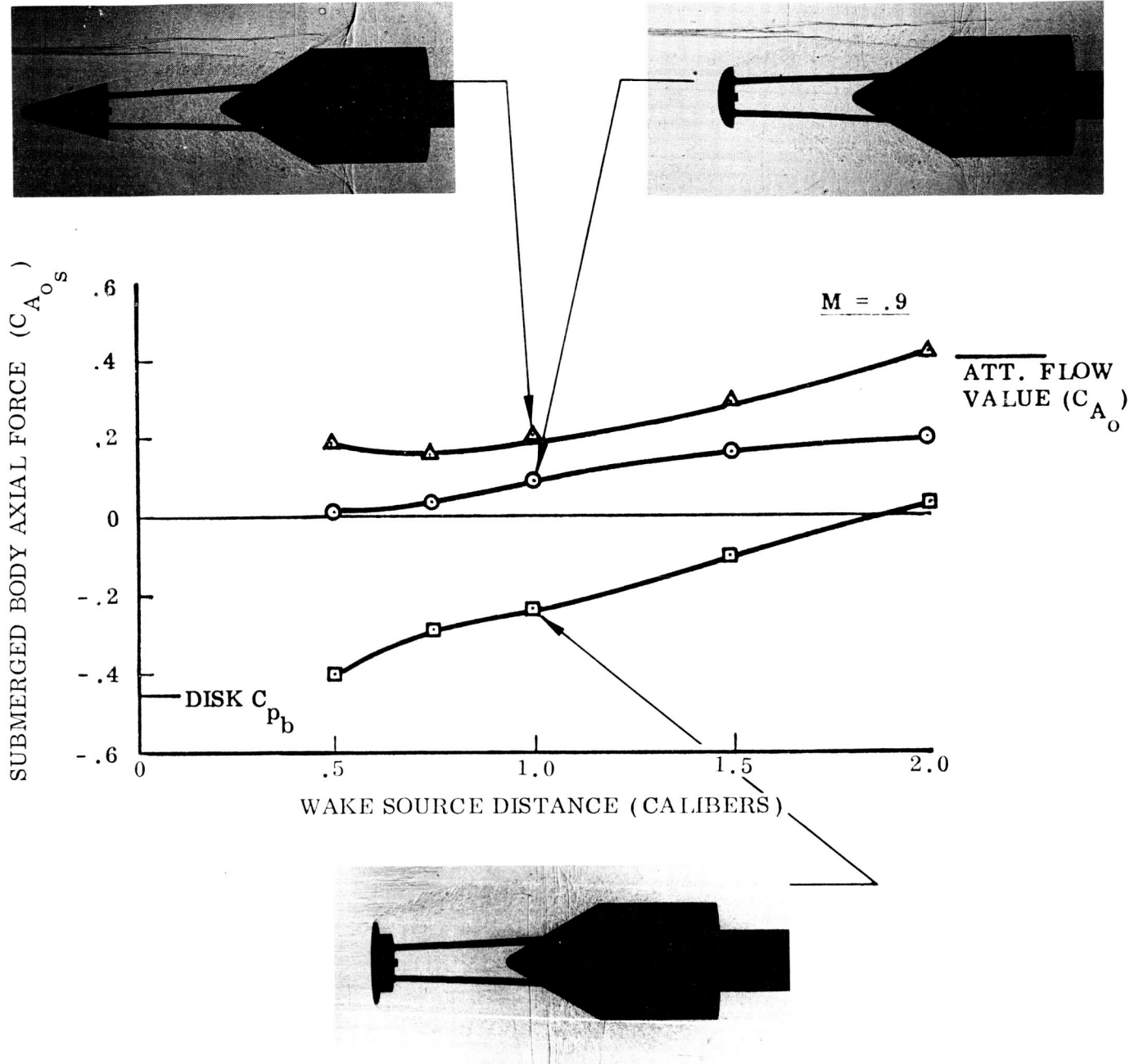


Fig. 3 Submerged Body Axial Force for Various Wake Sources ( $\alpha = 0$ )

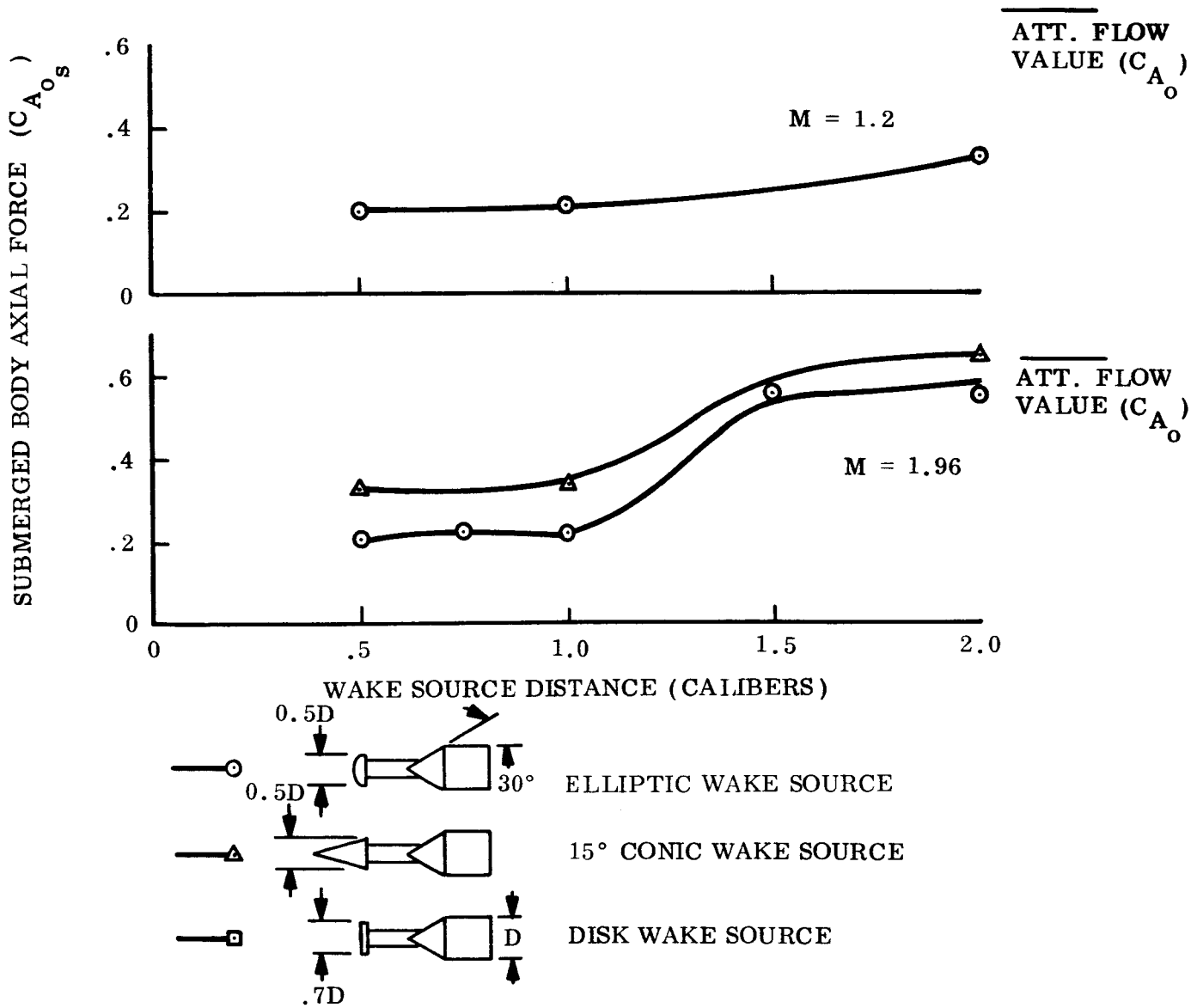


Fig. 3 (Continued)

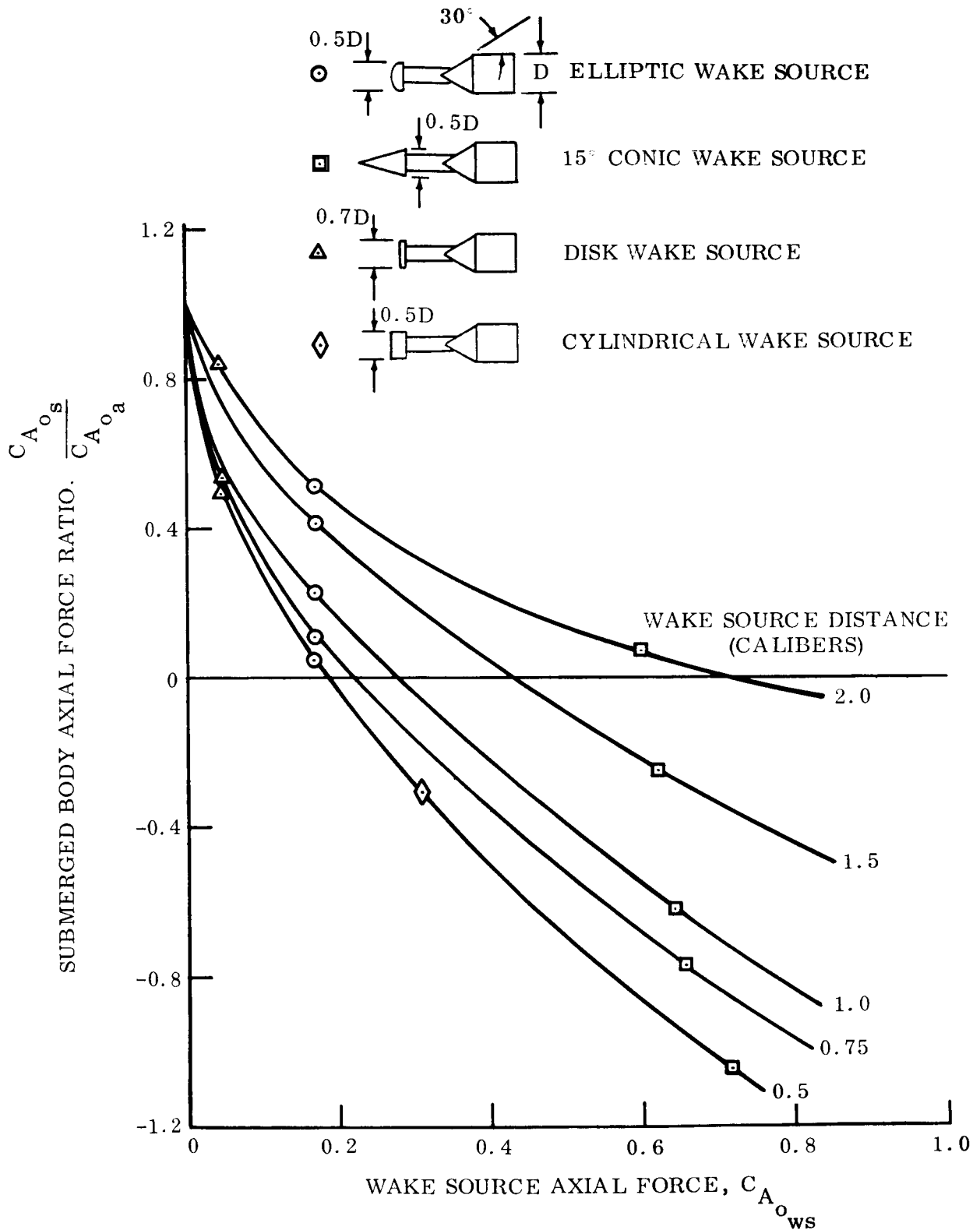


Fig. 4 Correlation of Submerged Body Axial Force Ratio With Wake Source Axial Force ( $M = 0.9$ )

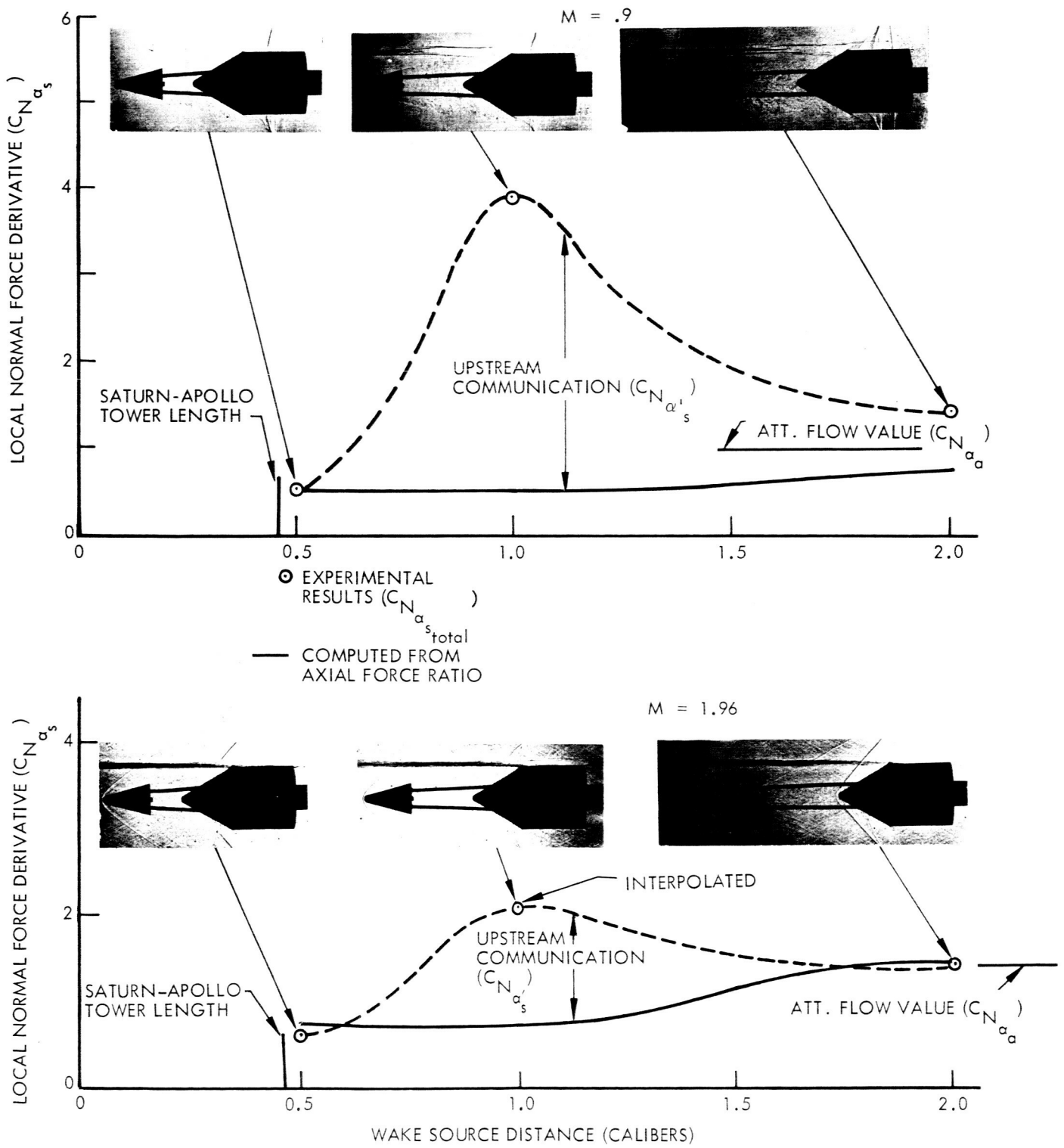


Fig. 5 Local Crossflow Effects on the Submerged Conic Forebody (Directing Wake Source)

on the aft body. It is worthy of note that the axial force ratio seems to be valid for the Saturn-Apollo geometry which justifies its application in Ref. 1.

Examination of the accompanying shadowgraphs indicate that the large increase in the local derivative occurs when the wake closes on the submerged body. For tower lengths shorter than this critical length the presence of the submerged body opens the wake moving reattachment aft of the shoulder. Thus, the submerged body is completely engulfed in separated flow and pitching the body in no way alters the wake geometry. For wake source distances in the critical range the wake closes on the submerged body and pitching the body alters the reattachment conditions increasing the windward reattachment pressure and decreasing the leeward pressure. The effect of changing the reattachment conditions is propagated upstream through the reverse flow region changing conditions at the wake source and causing the wake to be translated further to the leeward side. The tendency for the windward reattachment to move forward toward the cone apex as the wake is translated over the submerged body is counteracted by the increased return mass flow in a reduced stream tube tending to expand the windward wake. On the leeward side the tendency for the reattachment zone to move toward the shoulder is countered by reduced return mass flows in an increasing stream tube; thus the wake translation due to submerged body attitude is stabilized. As the wake source distance is increased the wake closes forward of the submerged body cutting off any forward

propagation effects\* and the experimental data converge toward the predictions obtained using the axial force ratio.

That the submerged body has an effect on conditions at the wake source is indicated in Fig. 6. The effect of the submerged body on wake source base pressure diminishes approaching the free wake value as the wake source distance increases. At subsonic Mach numbers the base pressure reduction with wake source distance is not as rapid as for supersonic Mach numbers which correlates with the less rapid convergence at  $M = .9$  of the experimental data and predicted normal force values shown in Fig. 5. While the wake source base pressure variation indicates that upstream communication exists, it is not indicative of the sensitivity of wake source conditions to changes of the reattachment conditions. Figure 7 presents,  $\partial C_{pb} / \partial \alpha$ , the rate of change of wake source base pressure with the angle of attack of the wake source-submerged body combination, as a function of wake source distance. Since the wake source is non-directing in this case (as will be shown later) this represents the combined effects of  $\alpha_s$  and  $\beta$ , i.e.,  $\partial C_{pb} / \partial \alpha = \partial C_{pb} / \partial \alpha_s + \partial C_{pb} / \partial \beta$ . The deviation of the base pressure derivative from the free wake value correlates with the increased local derivative for critical wake source distances (Fig. 7), thus giving further evidence that this is indeed an upstream communication effect. The accompanying shadowgraphs verify that the increased normal force is due to sweeping the wake further to the leeward side.

---

\* The shadowgraphs in Fig. 5 show a shock in the wake forward of the submerged body at  $M = 1.96$  and a wake source distance of 2.0 calibers which indeed isolates the wake source from any upstream communication effects.

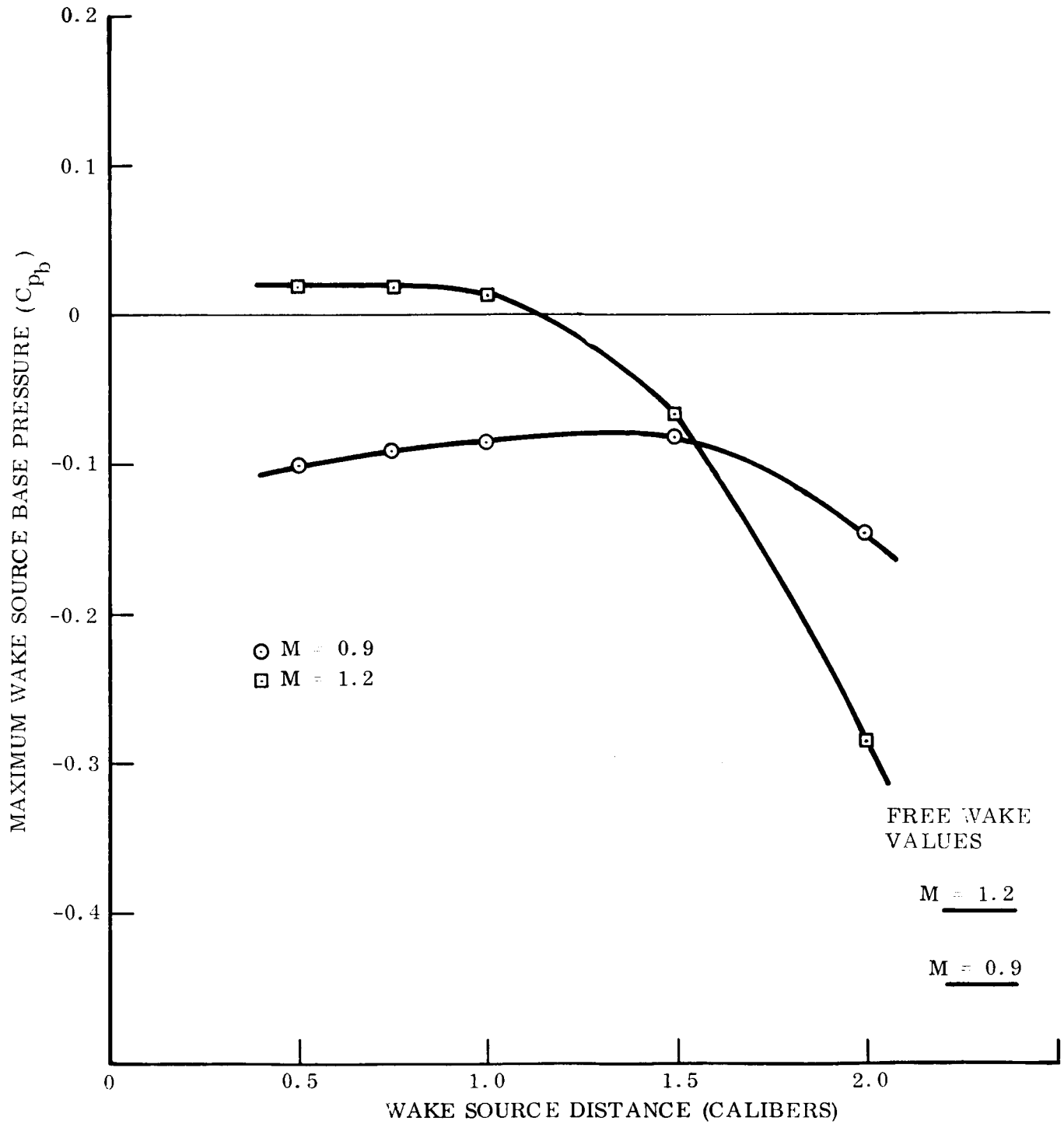


Fig. 6 Effect of the Submerged Body on the Maximum Wake Source Base Pressure (Elliptic Wake Source)



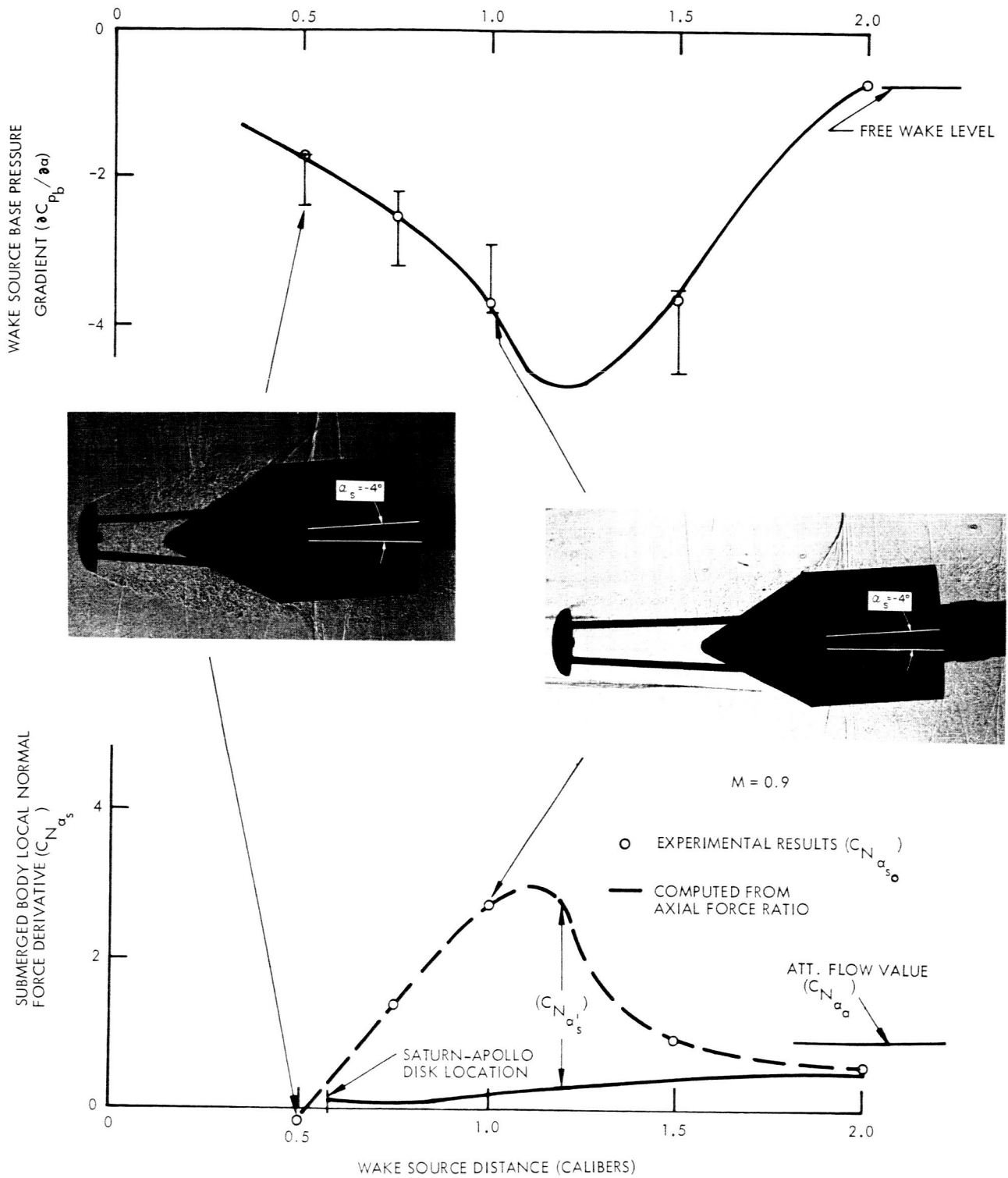


Fig. 7 Correlation of Wake Source Base Pressure Sensitivity With Submerged Conic Forebody Local Loads

WAKE SOURCE DISTANCE (CALIBERS)

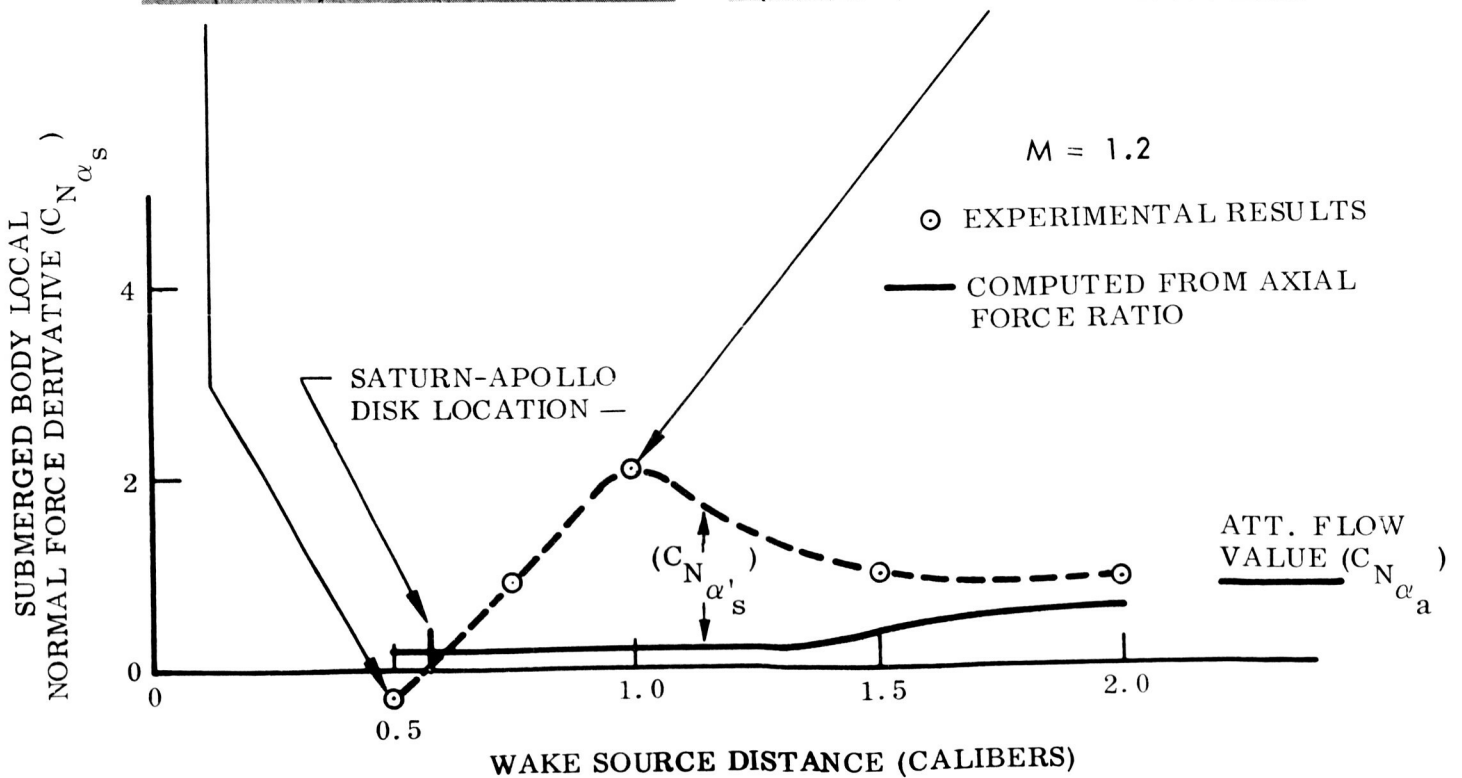
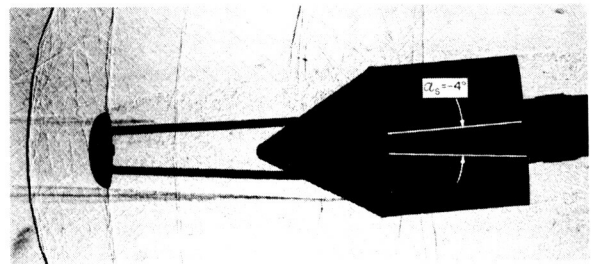
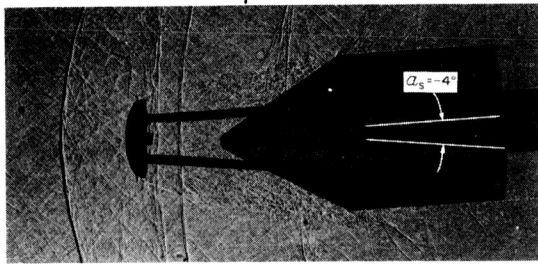
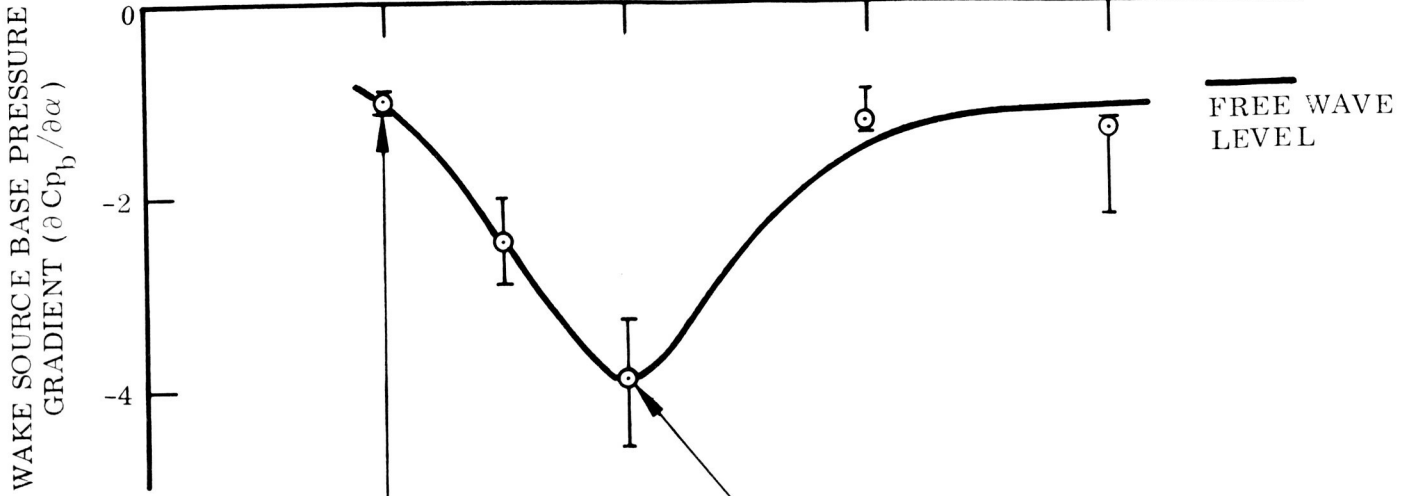
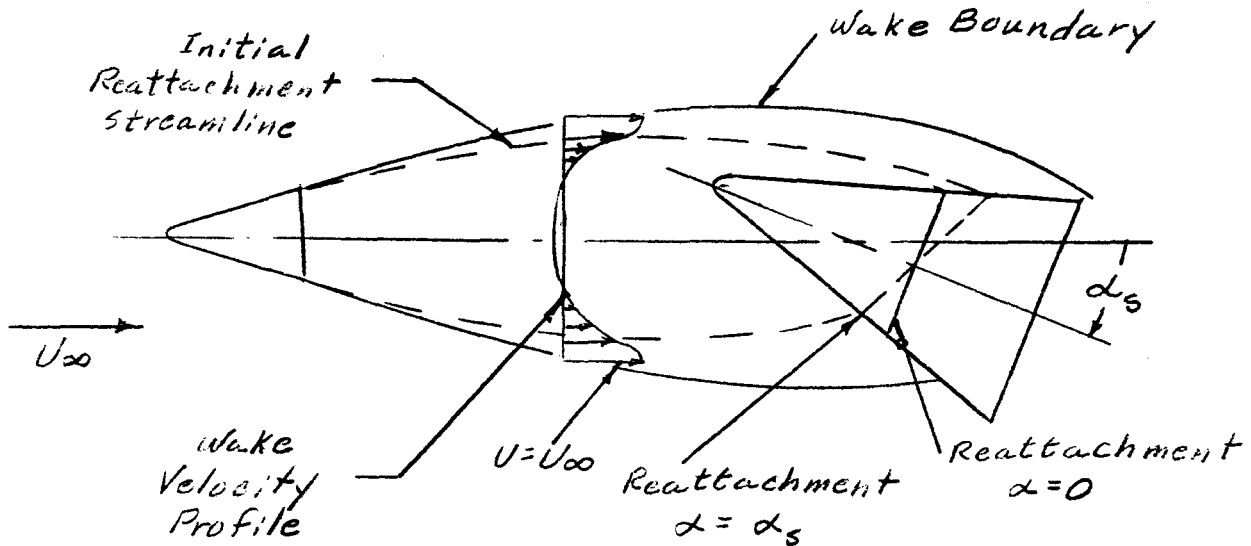


Fig. 7 (Continued)

The deviation in the local load is then due to the relative windward to leeward side variations of the reattachment conditions being propagated upstream and flipping the wake to the leeward side. Reattachment, as used here, refers to the impingement of the outer high velocity portion of the wake flow on the submerged body as shown in Sketch 1.



Sketch 1

Pitching the submerged body causes the initial reattachment streamline to move forward on the windward side and aft on the leeward. If the wake is approximated by a series of constant velocity streamtubes it becomes evident that this shifting occurs throughout the reattachment zone. This will result in a windward to leeward side pressure differential in addition to the usual differential caused by the variation in flow turning at angle of attack. The pressure differential will in turn produce a vertical velocity component within the wake that, when propagated forward to the wake source, will produce

the observed flipping of the wake to the leeward side. The magnitude of the vertical velocity will of course vary with the submerged body configuration as will the reverse mass flow rate. When the wake is translated over the submerged body the resulting vertical velocity component results entirely from the shifting of the reattachment zone. It becomes apparent from the foregoing discussion that the additional normal force will be a maximum when reattachment occurs on the submerged body; thus, maximizing the vertical wake velocity (because of the large velocity gradients in the outer wake flow) and the recirculation mass flow (due to the turning back of higher velocity flow). Conversely, these effects diminish when the submerged body is exposed to the low velocity gradients and small recirculation mass flow rates (both of which characterize the flow at wake source distances outside the critical range).

The additional normal force is then the result of a vertical wake velocity component being communicated upstream to the wake source. The vertical velocity is related to the submerged body normal force, and the upstream communication is a function of the reattachment pressure. The reattachment pressure is a function of the submerged body geometry as well as the wake conditions since it increases with the body slope at reattachment. The axial force moment is indicative of the reattachment pressure rise as affected by both the submerged body geometry and the wake properties (Ref. 11). The axial force moment on a cone may be related to the normal force as follows;

$$C_{ax} = \frac{C_n}{L} \int_0^L C_n \sin \theta \, dx$$

where  $\bar{D}$  is the diameter at the centroid of the pressure distribution and  $\theta$  is the cone half-angle. Both the vertical velocity and the upstream communication are then related to the normal force. In the first order approximation it has, therefore, been assumed that

$$\frac{\partial z}{\partial \alpha} = \left( \frac{\partial z}{\partial C_N} \right) \left( \frac{\partial C_N}{\partial \alpha} \right) = C_{N\alpha} \frac{\partial z}{\partial C_N} \quad (6)$$

where for submerged body rotation

$$C_{N\alpha} = C_{N\alpha S}$$

The total load on the submerged body due to local rotation is thus

$$C_{N\alpha ST} = C_{N\alpha S} + \Delta^i C_{N\alpha Z} \frac{\partial z}{\partial \alpha} \alpha_S$$

and

$$C_{N\alpha ST} = C_{N\alpha S} + \Delta^i C_{N\alpha Z} \frac{\partial z}{\partial \alpha}$$

for the assumed variation of  $z$  with  $\alpha$ . Substituting Equation (6) into the above gives

$$C_{N\alpha ST} = C_{N\alpha S} + \Delta^i C_{N\alpha Z} \frac{\partial z}{\partial C_N} C_{N\alpha S}$$

However,  $z = r\beta$ , therefore,

$$C_{N\alpha ST} = C_{N\alpha S} \left( 1 + \Delta^i C_{N\alpha \beta} \frac{\partial \beta}{\partial C_N} \right) \quad (7)$$

Likewise an additional translation of the wake,  $\Delta z$ , occurs as the result of the vertical wake velocity produced by an initial wake source translation,  $z$ .

$$\Delta z = \frac{\partial z}{\partial C_N} \Delta^i C_N \quad (8)$$

where  $\Delta^i C_N$  is the initial wake induced translatory force coefficient, and

$$\Delta^i C_N = \Delta^i C_{N\alpha} z$$

The total translatory normal force is

$$\Delta^i C_{N_T} = \Delta^i C_{N_Z} (z + \Delta z) = \Delta^i C_{N_Z} \left[ z + \left( \frac{\partial z}{\partial C_N} \Delta^i C_{N_Z} \right) z \right] \quad (9)$$

and

$$\Delta^i C_{N_{\beta_T}} = \Delta^i C_{N_{\beta}} \left( 1 + \Delta^i C_{N_{\beta}} \frac{\partial \beta}{\partial C_{N_{\beta}}} \right) \quad (10)$$

since  $z = l\beta$ .

The wake directing derivative is simply a translating derivative caused by the wake source imparting an initial inclination to the wake centerline.

Thus

$$z = \frac{\partial z}{\partial \theta} \theta \quad (11)$$

The total wake directing load is then

$$\begin{aligned} \Delta^i C_{N_T} &= \Delta^i C_{N_{\theta}} (\theta + \Delta \theta) \\ &= \Delta^i C_{N_{\theta}} \left( \theta + \frac{\partial \theta}{\partial z} \Delta z \right) \end{aligned}$$

substituting Equations (8), (9), and (11) into the above and differentiating (remembering that  $z = l\beta$ ),

$$\Delta^i C_{N_{\beta_T}} = \Delta^i C_{N_{\beta}} \left( 1 + \Delta^i C_{N_{\beta}} \frac{\partial \beta}{\partial C_{N_{\beta}}} \right) \quad (12)$$

From Equations (7), (10) and (12) the initial (computed from axial force ratio) to total derivative ratios may be related for a given wake source distance as follows:

$$\frac{C_{N_{\beta_T}}}{C_{N_{\beta}}} = \frac{\Delta^i C_{N_{\beta_T}}}{\Delta^i C_{N_{\beta}}} = \frac{\Delta^i C_{N_{\theta}}}{\Delta^i C_{N_{\theta}}} = \left( 1 + \Delta^i C_{N_{\beta}} \frac{\partial \beta}{\partial C_{N_{\beta}}} \right) = 1 + \epsilon \quad (13)$$

where  $\epsilon$  is a constant for a given Mach number, configuration, and wake source distance. Therefore, by knowing the initial and total derivatives for one load component (in this case  $C_{N\alpha} / C_{N\alpha_s}$ ) one may obtain the upstream communication effects for all derivatives. In this manner the upstream communication component of the translational derivative ( $\Delta^i C_{N\theta}$ ) was computed (Fig. 8). Large upstream communication effects are evident for critical wake source distances. Figure 9 presents similar data for the directing derivatives. Again strong upstream effects are indicated. The subsonic data (Fig. 9.) shows the elliptical wake source to be non-directing while the ellipse-cylinder wake source has directing effects opposite to those of a slender wake source, i.e.,  $\Delta^i C_{N\theta} > 0$ . Nose-induced separation occurs at the ellipse-cylinder juncture (Ref. 13) and the cylinder supplies sufficient length for the separation to "move"; thus, as the wake source is pitched separation increases on the leeward side and diminishes on the windward side causing the wake to be swept to the leeward side and thereby producing a positive  $\Delta^i C_{N\theta}$ . This is evident on the accompanying shadowgraphs as is the increased slender body wake directing for critical wake source distances.

Inherent in the axial force ratio prediction of the local derivative is the assumption of constant Mach number, or at least constant local force coefficient, throughout the wake. This obviously introduces some error into the predictions as shown in Figure 10 where the experimental data are actually less than the predictions for large separation distances. The corrected

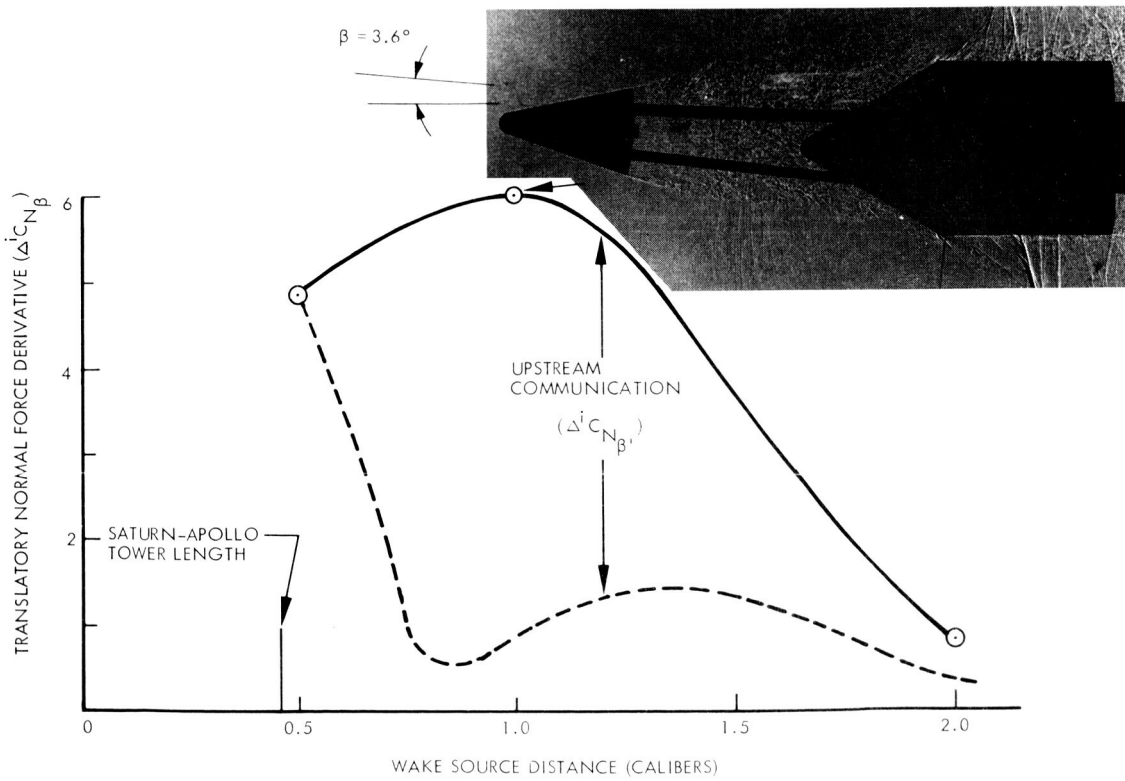
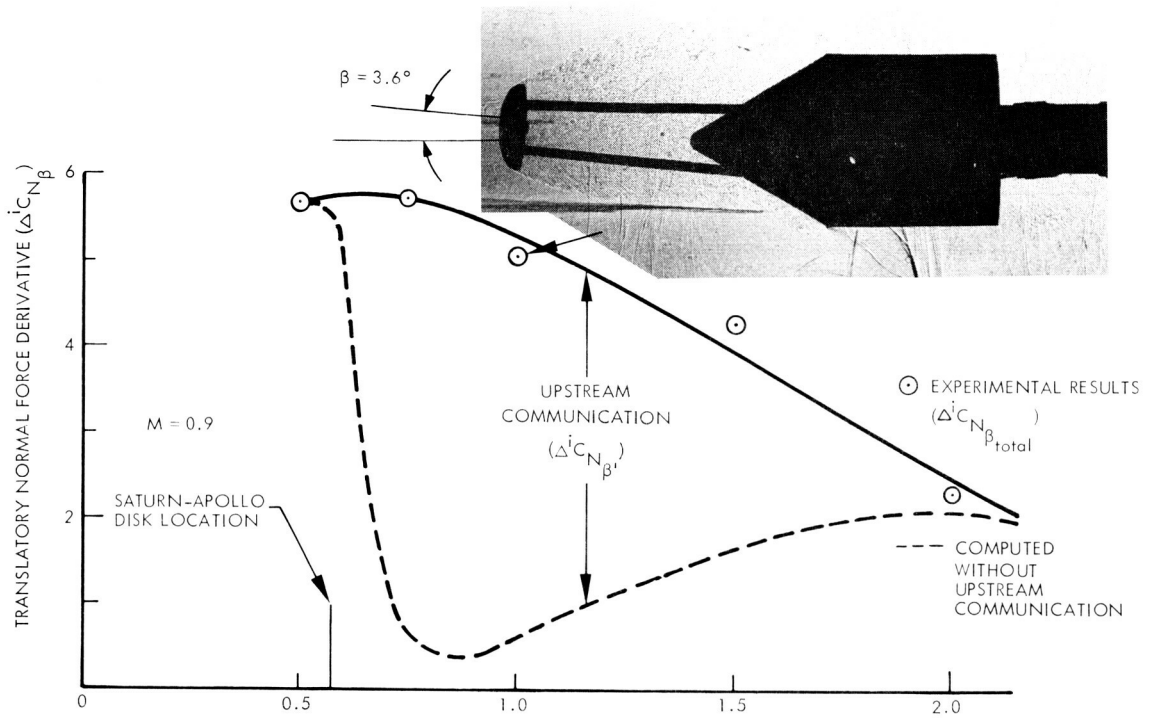


Fig. 8 Wake Translation Effects on the Submerged Conic Forebody



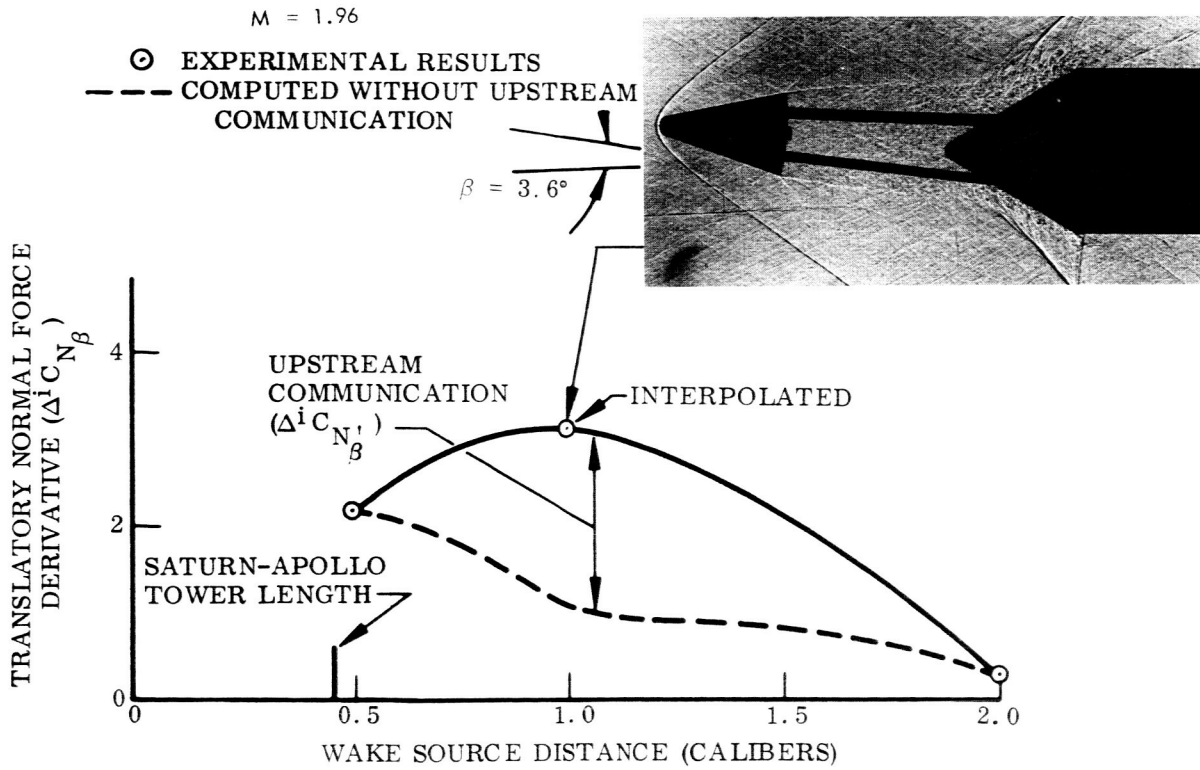
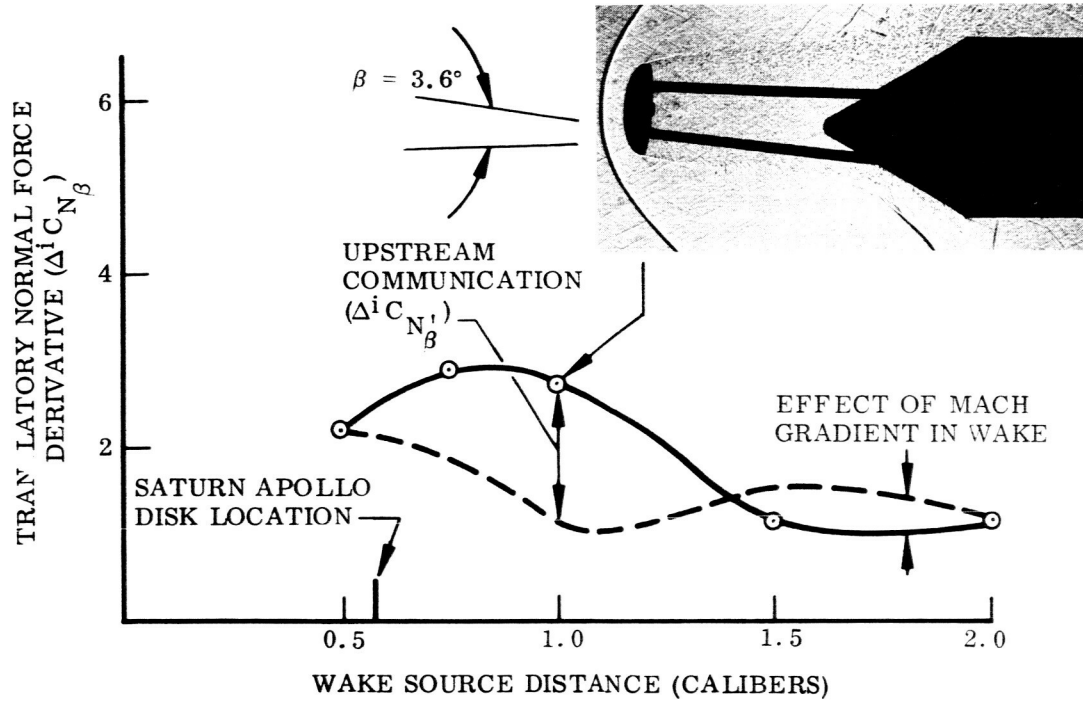


Fig. 8 (Continued)

M = .9

○ ELLIPTIC WAKE SOURCE

□ 15° CONE WAKE SOURCE

△ ELLIPSE - CYLINDER WAKE SOURCE

--- COMPUTED DIRECTING DERIVATIVE FOR 15° CONE WAKE SOURCE WITHOUT UPSTREAM COMMUNICATION

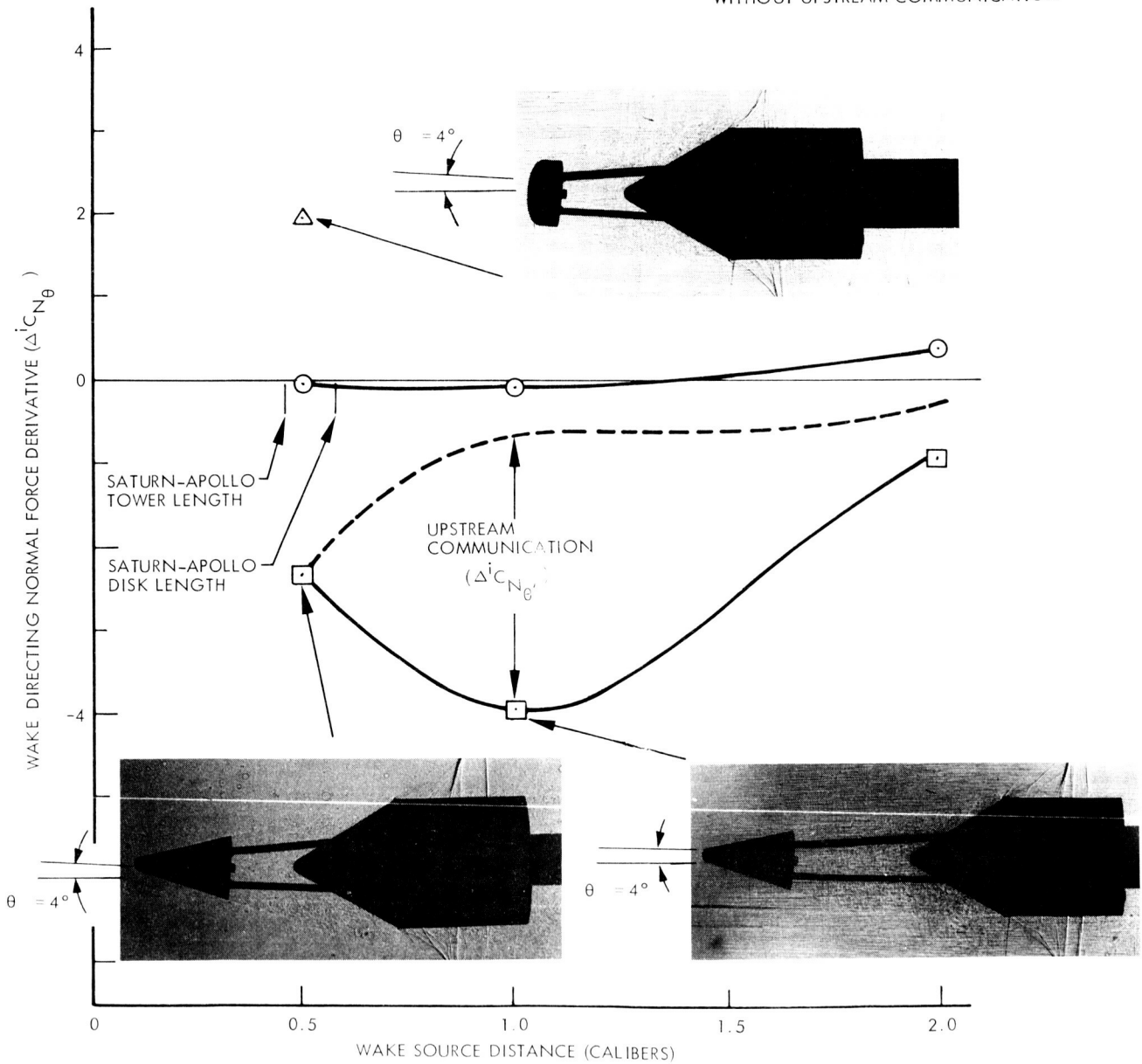


Fig. 9 Comparison of Wake Directing Effects on the Submerged Conic Forebody

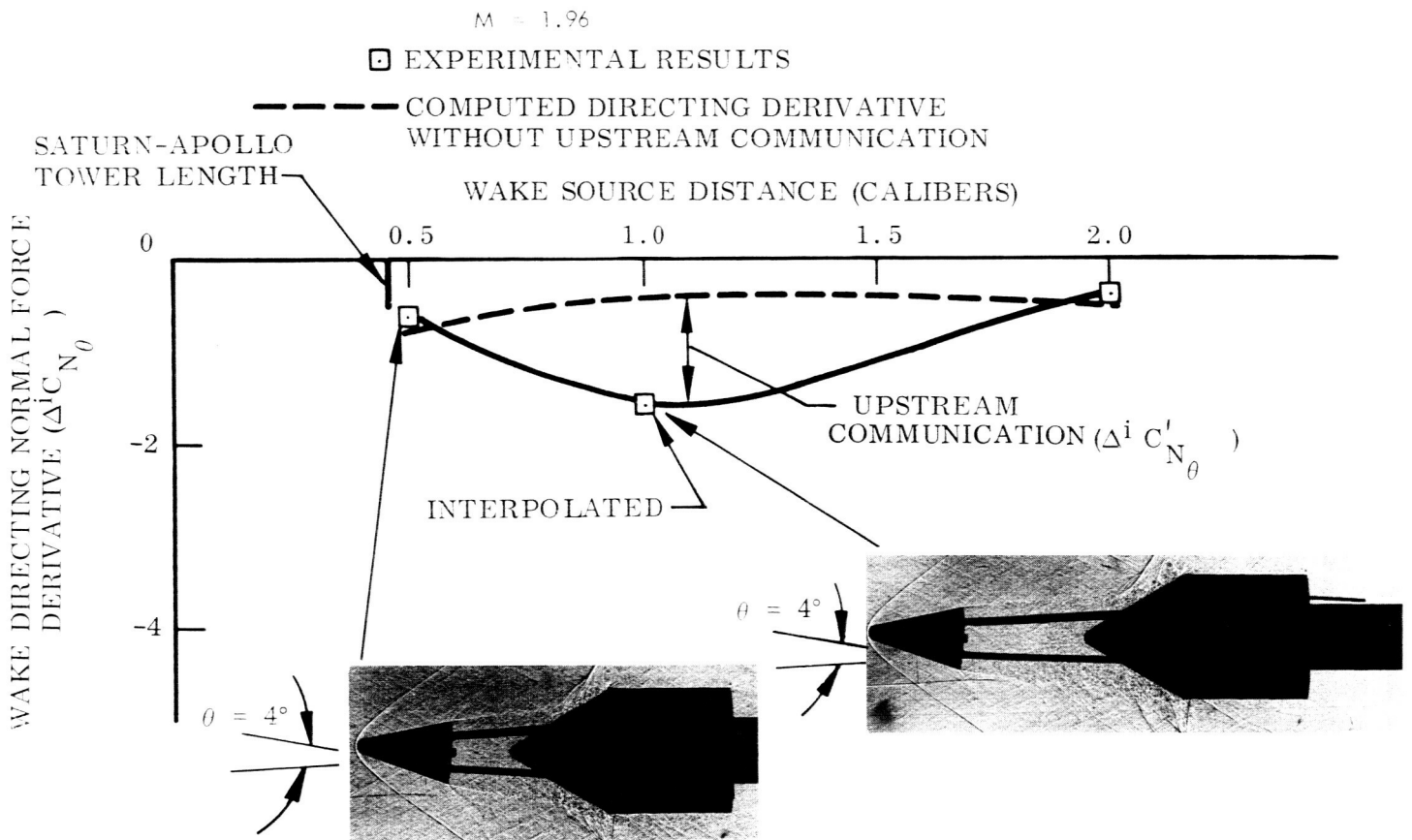


Fig. 9 (Continued)

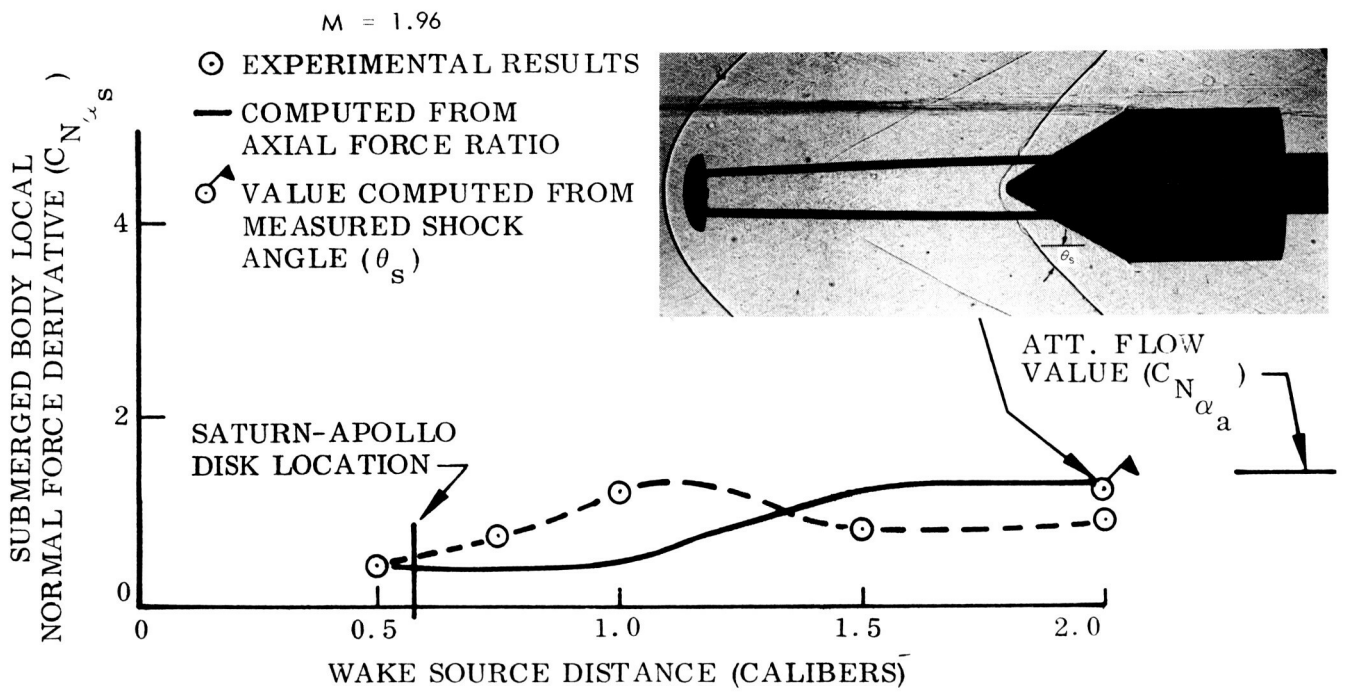


Fig. 10 Effect of Wake Mach Number Gradient

data point\* agrees rather well with predictions indicating the difference is indeed due to the Mach deficit. For the geometries considered herein, the effect appears to be of secondary importance judging by the usually good agreement between prediction and experiment outside the regions of large upstream influence. This effect will obviously diminish in importance as the submerged body to wake source diameter ratio increases.

The submerged body may also affect wake source forebody characteristics if separation occurs forward of the wake source base thereby allowing communication with the wake. It has been demonstrated that the submerged body has a large effect on wake source base pressure (Fig. 6). At  $M = 1.2$  a deviation between the total axial force on the wake source with and without a submerged body in the wake occurs as a result of these base pressure effects (Fig. 11). Likewise a portion of the total axial force deviation at  $M = .9$  also results from the submerged body affecting the wake source base pressure. However, at  $M = .9$  a difference in the forebody axial force with and without a body in the wake was observed. This occurs because the boundary layer just forward of the base is weak and just about to separate, and the increase in base pressure due to the pressure of the body submerged in the wake is sufficient to force separation to occur forward of the base. This causes the ordinarily negative pressure field on this portion of the ellipse (Ref. 15)

---

\* The correction was made by measuring the shock angle in the wake ( $\theta_S$ ) and consulting Ref. 12 and 13 to obtain the correct Mach number and force derivative, respectively.

ATTACHED FLOW LEVELS  
 TOTAL FOREBODY  
 AXIAL FORCE

○ M = 0.9  
 □ M = 1.2

NOTE: FLAGGED SYMBOLS AND  
 DASHED LINES DENOTE  
 FOREBODY AXIAL FORCE

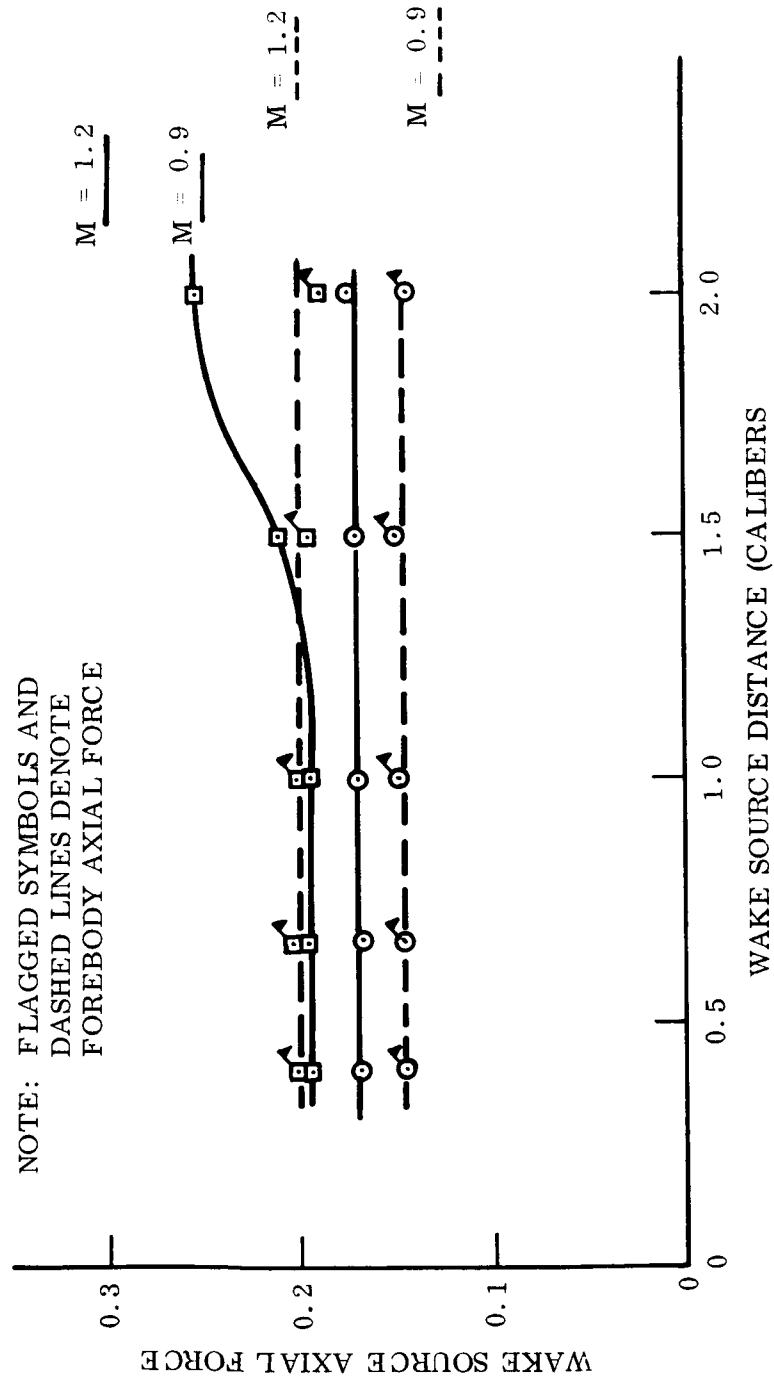


Fig. 11 Effect of Submerged Body Proximity on Wake Source Axial Force  
 (Elliptic Wake Source)

to become more positive increasing the forebody axial force. When the total wake-source submerged-body combination is pitched this upstream effect of the submerged body becomes stronger on the windward side (due to the  $\beta$  deflection) causing the windward side to experience greater pressures thus increasing the wake source normal force. These effects, of course, diminish with wake source distance as shown in Figure 12.

The experimental data have produced evidence that substantiate the veracity of the rather uncomplicated techniques applied to the Saturn-Apollo vehicles. They have also indicated that for other geometries strong upstream effects occur that drastically alter the loads on both the submerged body and the wake source.

#### Aft Cylinder Loads

In the analysis of the Saturn vehicles it was discovered that separation quite often passed over the shoulder of a sloping surface and attached on the aft cylinder (Ref. 1 & 2). The effect of increased crossflow angle at the separation source was to increase the leeward side separation thus allowing more of the reattachment pressure rise to propagate forward to the shoulder. The leeward shoulder pressure was therefore increased while the corresponding windward pressure was reduced due to opposite effects. The result was a negative induced shoulder load. The local shoulder load was either positive or negative depending upon whether reattachment occurred initially forward or aft of the shoulder. Due to the limited extent of this test program detailed load distribution data were not obtained on

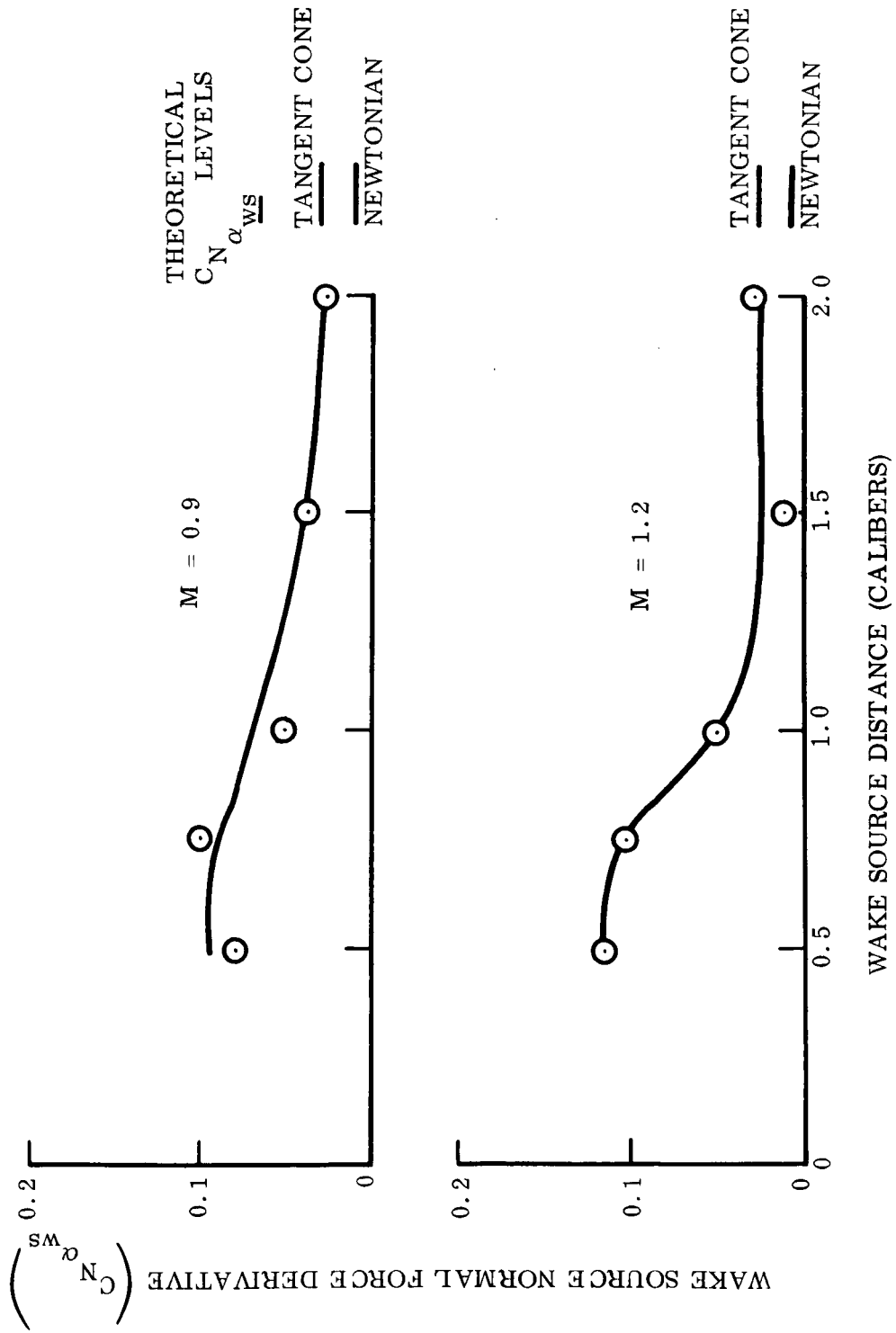


Fig. 12 Effect of Submerged Body Proximity on Wake Source Normal Force Derivative (Elliptic Wake Source)



the cylinder aft of the conical submerged body. It was possible, however, to obtain some pertinent information from the total load on the one caliber long aft cylindrical segment.

The local crossflow load on the aft cylinder evidently has a negative component as illustrated in Fig. 13 which shows the total aft cylinder load to be less than for attached flow. The center of pressure data (Fig. 14), when considered with the force data, also indicate that a force couple is acting on the submerged body. The forward center of pressure at  $M = .9$  for a total negative cylinder load could only be realized in the presence of a force couple. The aft positive component produces a larger moment than the negative load (in spite of the larger magnitude of the latter load) by virtue of its longer lever arm. The result is a negative moment and a total negative load producing the forward center of pressure. The far aft center of pressure locations for a positive total load shown at  $M = 1.96$  are also indicative of this type of force couple. A very small portion of the negative load just aft of the shoulder may propagate forward onto the cone causing the forward center of pressure shift shown in Fig. 15\*.

That the translational shoulder load is negative (as postulated in Ref. 1) may be seen in Fig. 16. The center of pressure data (Fig. 17) indicate

---

\* It should be noted that the center of pressure should normally be somewhere between the attached flow value and the  $1/2 \tan \theta$  (where  $\theta$  is the cone  $1/2$  angle) due to the velocity deficit in the wake core. The latter value (derived in Ref. 16) corresponds to an equivalent bubble wake model with reattachment at the cone shoulder.

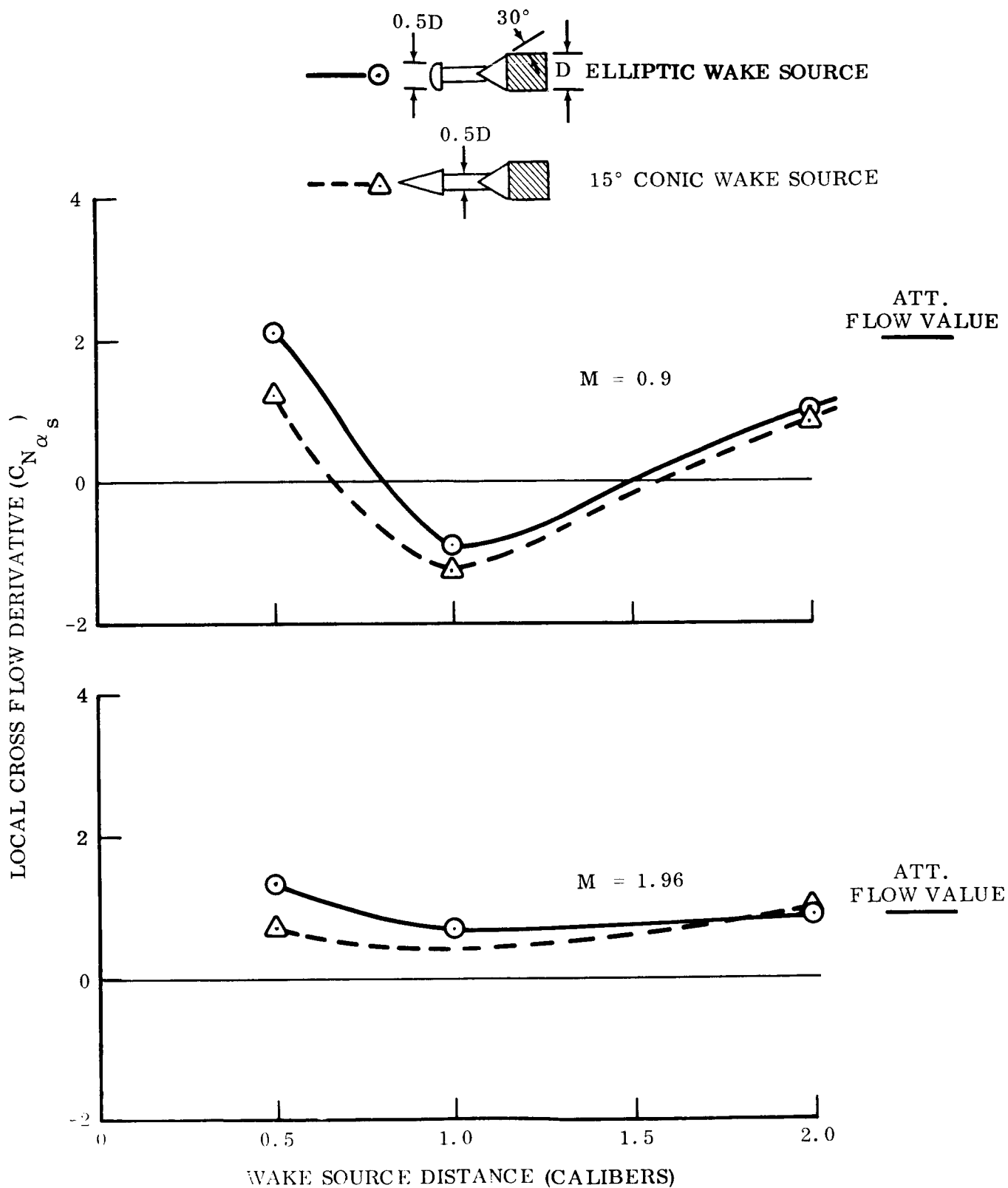


Fig. 13 Aft Cylinder Local Loads

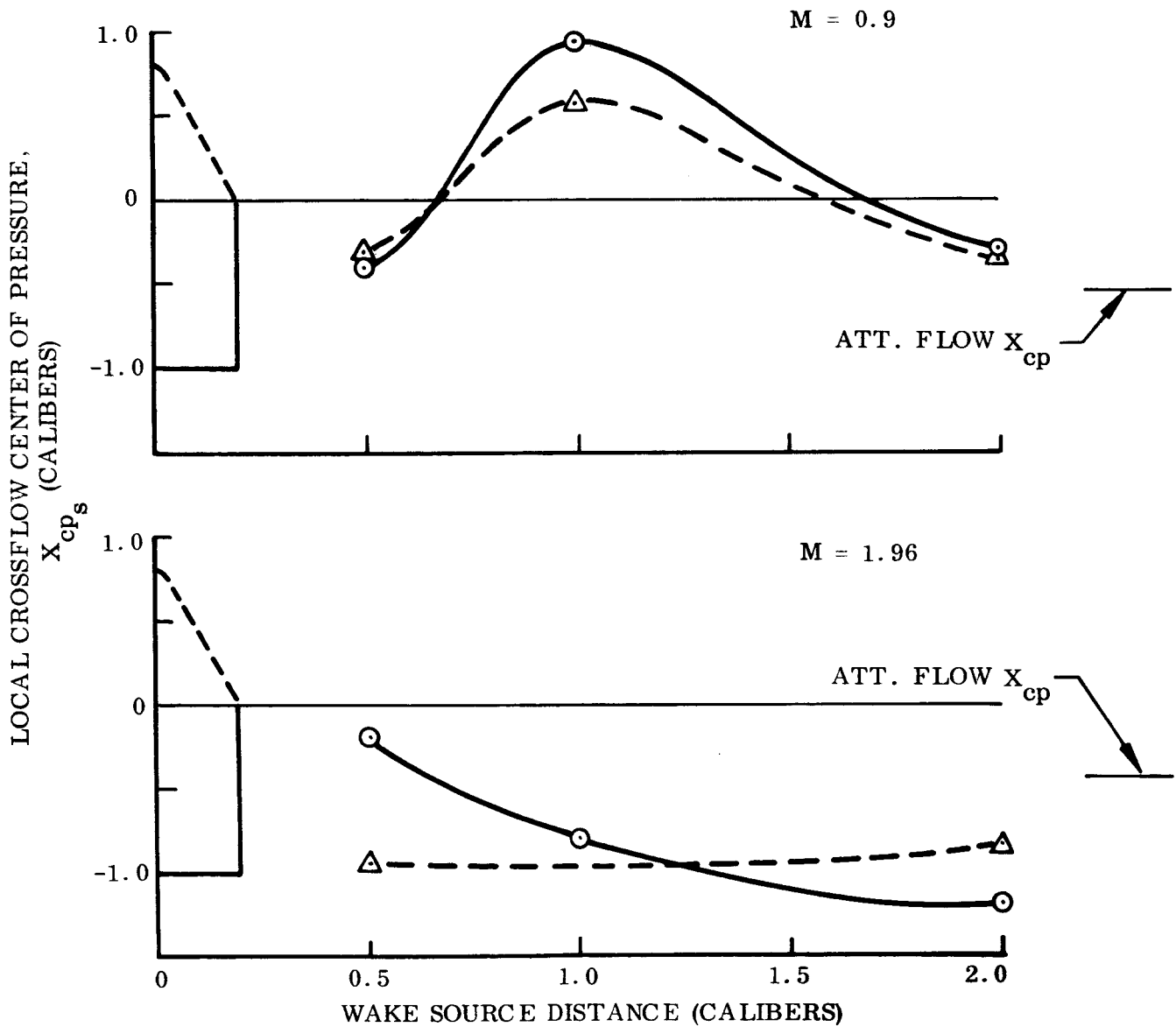
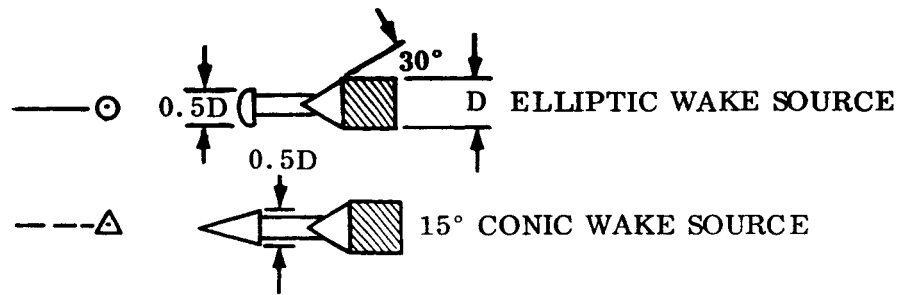


Fig. 14 Aft Cylinder Local Crossflow Center of Pressure

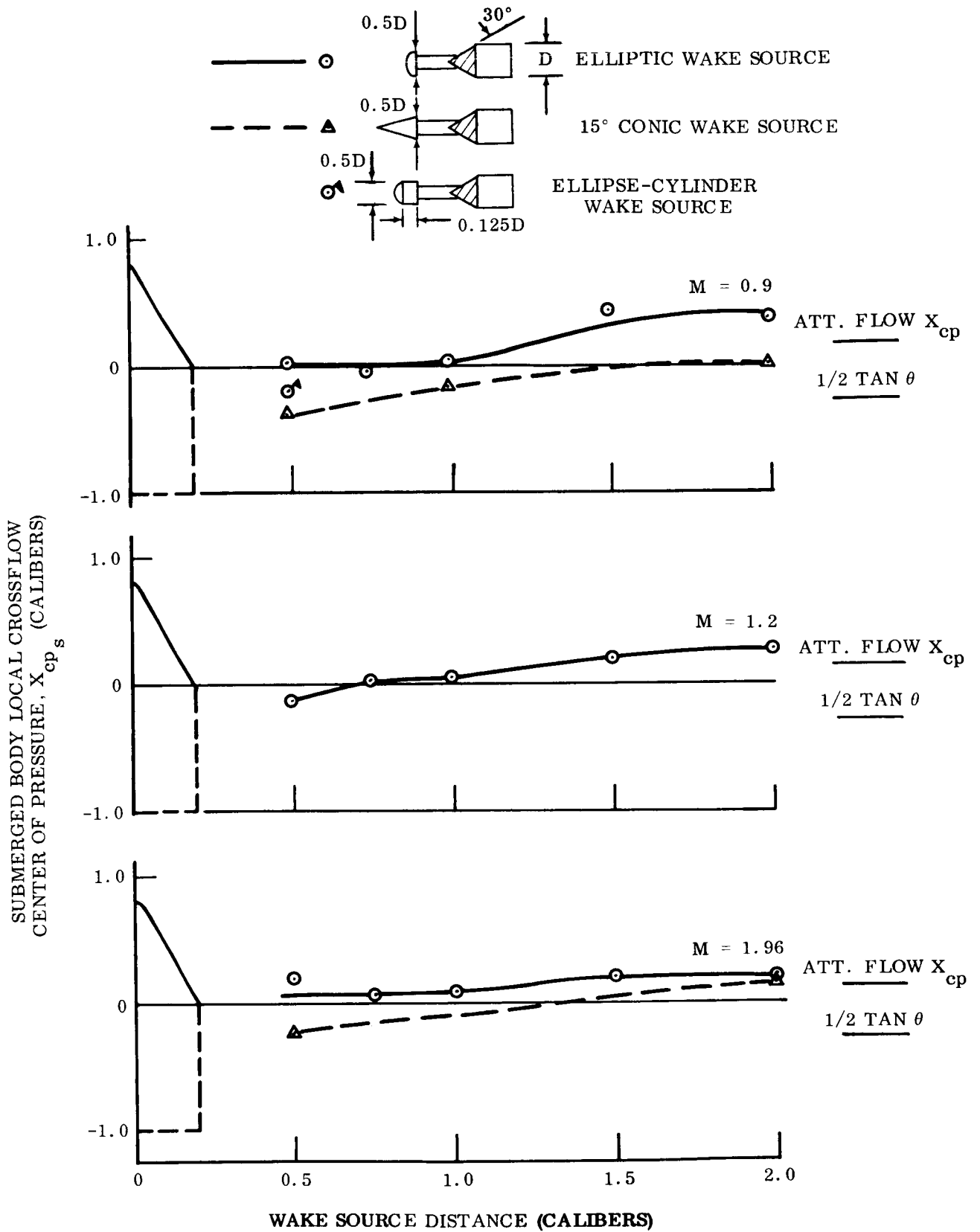


Fig. 15 Submerged Conic Forebody Local Crossflow Center of Pressure

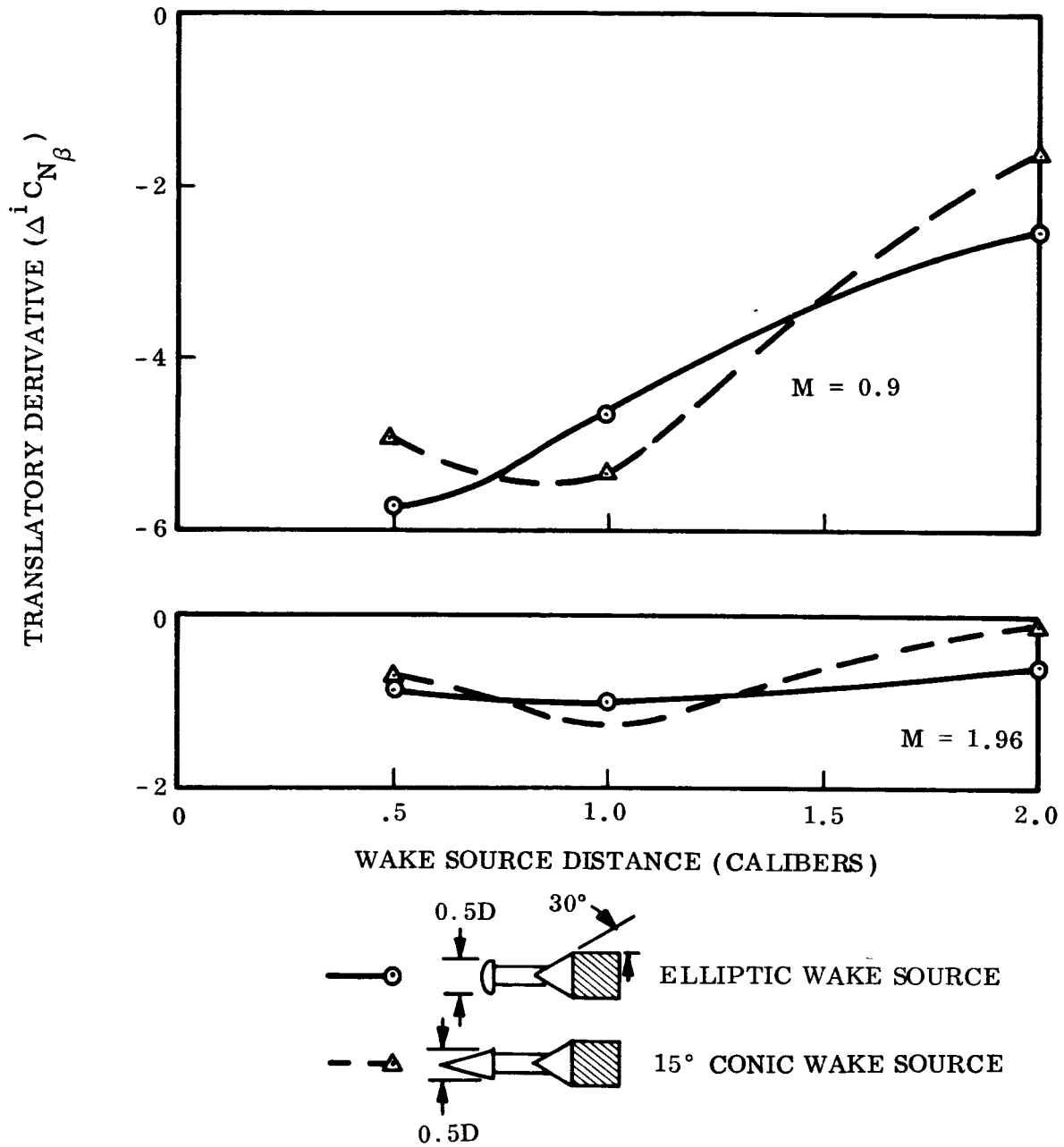


Fig. 16 Wake Translation Effects on Aft Cylinder Loads

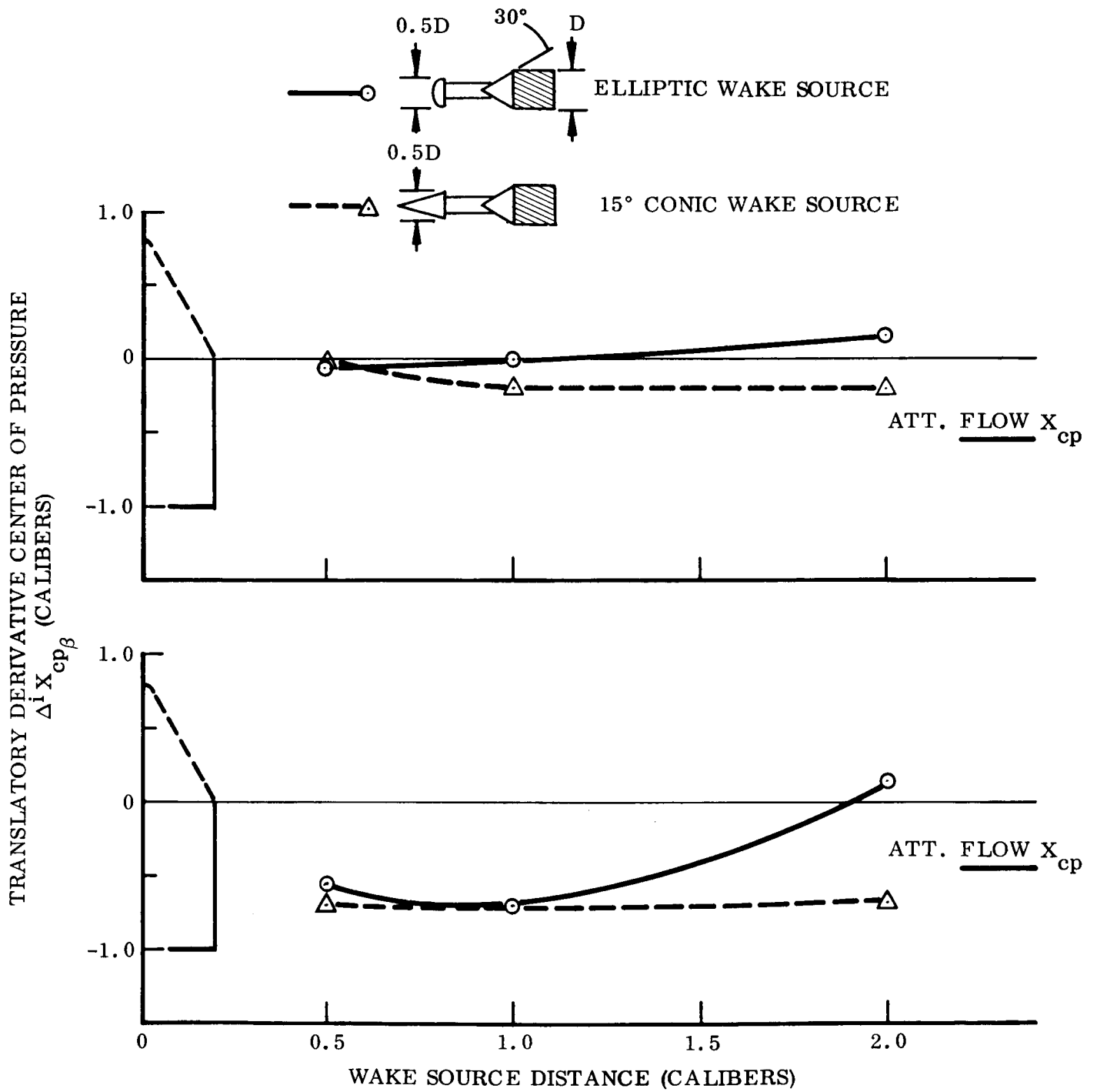


Fig. 17 Wake Translation Effects on Aft Cylinder Center of Pressure

that part of this induced load must also be positive. This is the result of the downstream reattachment pressure rises. These effects must be small, however, since the total induced load is negative and rather large, and the center of pressure irregularities are small (Fig. 17). There is also some evidence of the forward feeding effect (Fig. 18). The forward shift of the center of pressure on the cone is the result of the effective wake core contracting as the induced loads approach zero.

Figures 19 and 20 indicate that the directing derivative on the shoulder, like the translational load, is opposite in sense to its counterpart on the cone. Therefore, the slender wake source induces a positive shoulder load while the ellipse-cylinder induces a negative load. Again a forward shift in the center of pressure data (see Fig. 21 also) occurs as the induced load approaches zero.

The data tend to substantiate the theories of Ref. 1. The induced shoulder loads are of opposite sign to the preceding cone loads. The translational load has a small positive component that was recognized but neglected previously (with some justification since they are indeed small). The directing derivatives undoubtedly have similar effects. The shoulder loads also must have upstream communication components as evidenced by the shape of the load variation with wake source distance. The absence of detailed pressure distribution data preclude illustrating these effects quantitatively.

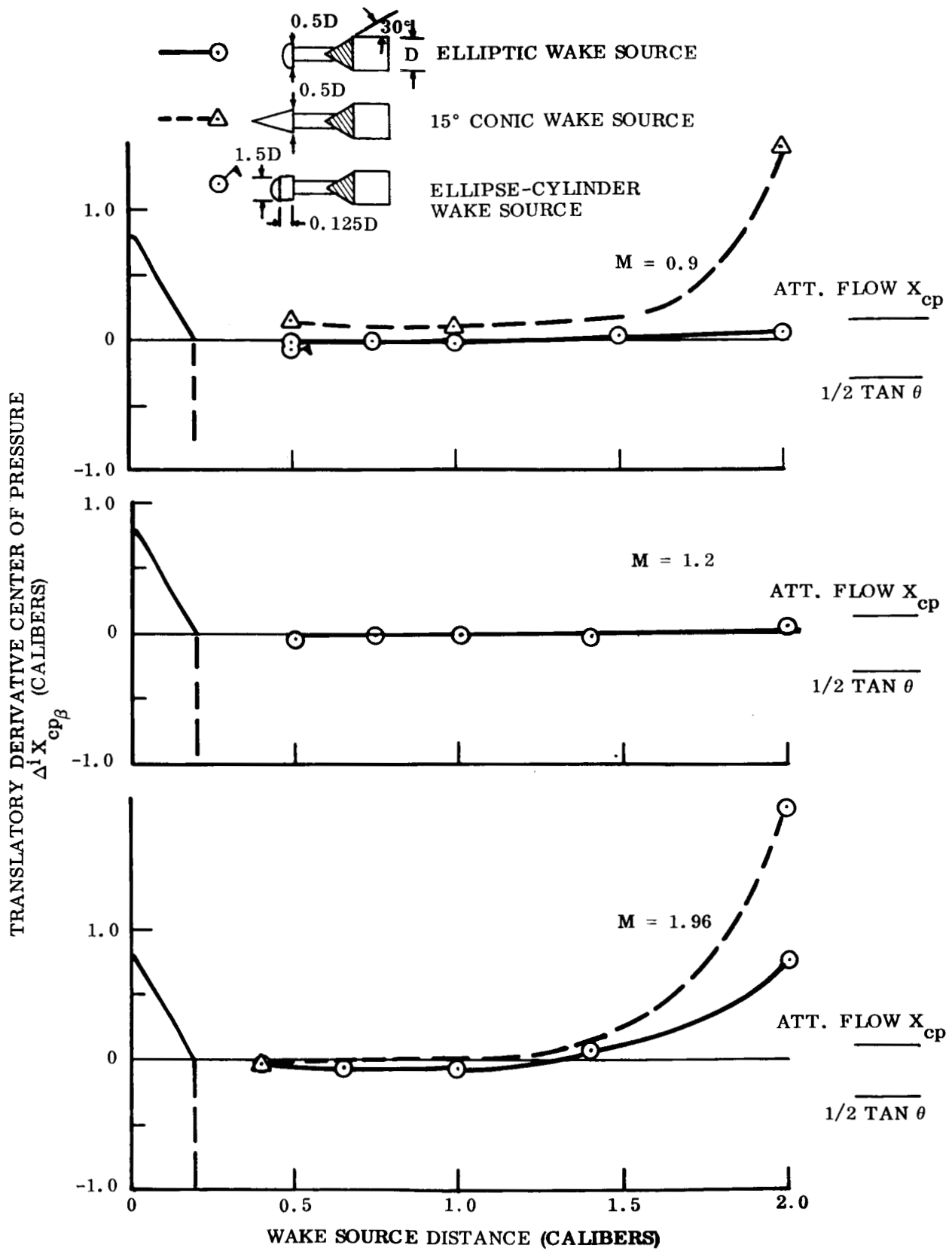


Fig. 18 Wake Translation Effects on the Submerged Conic Forebody Center of Pressure



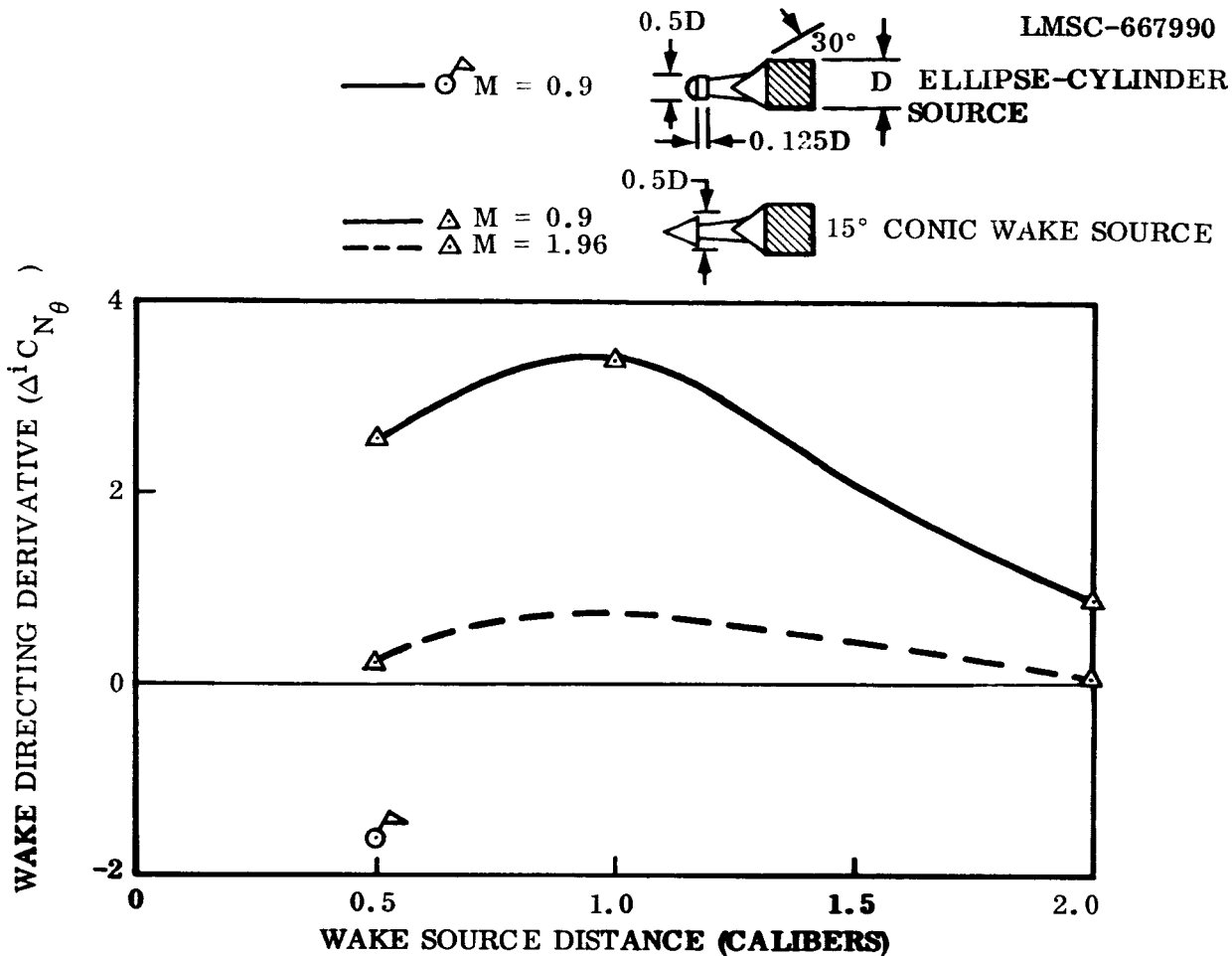


Fig. 19 Wake Directing Effects on the Aft Cylinder Load

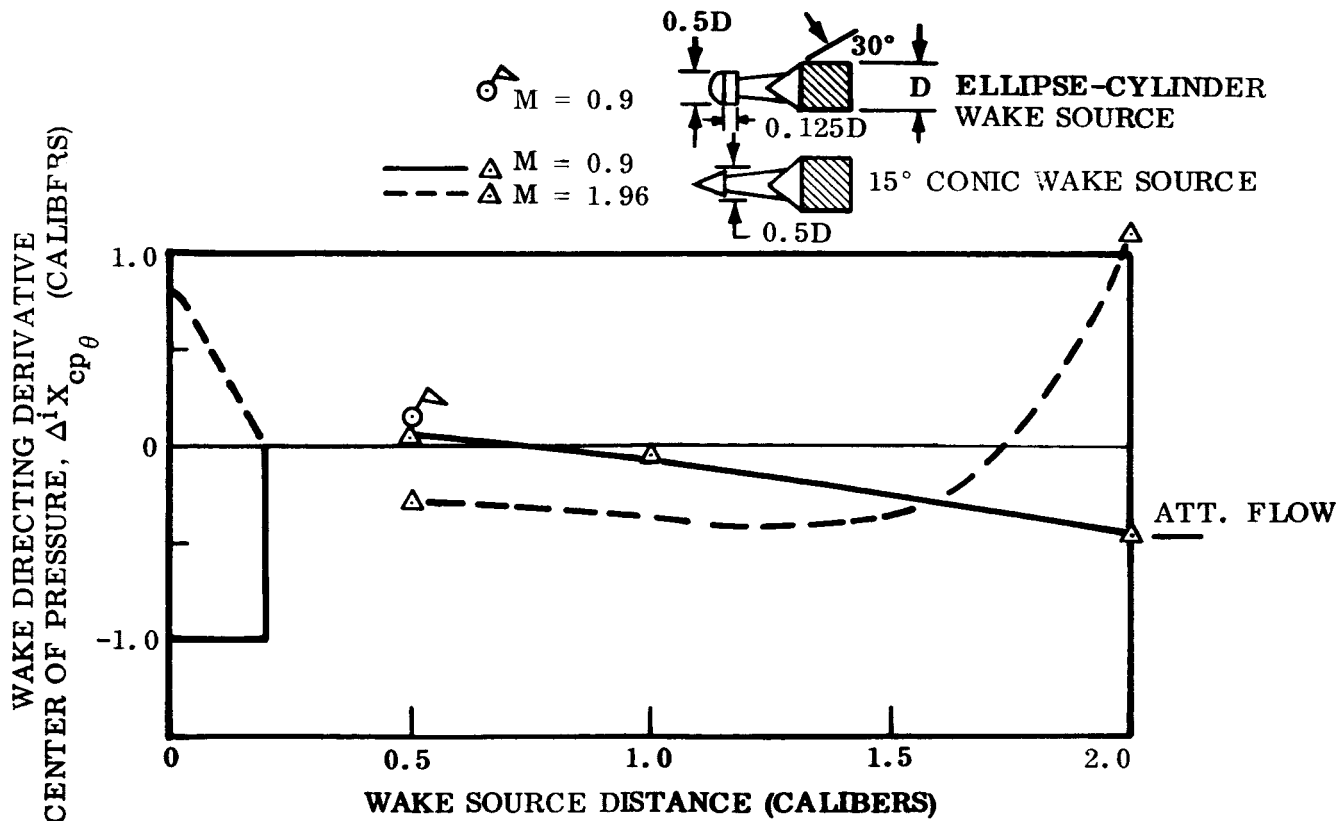


Fig. 20 Wake Directing Effects on the Aft Cylinder Center of Pressure

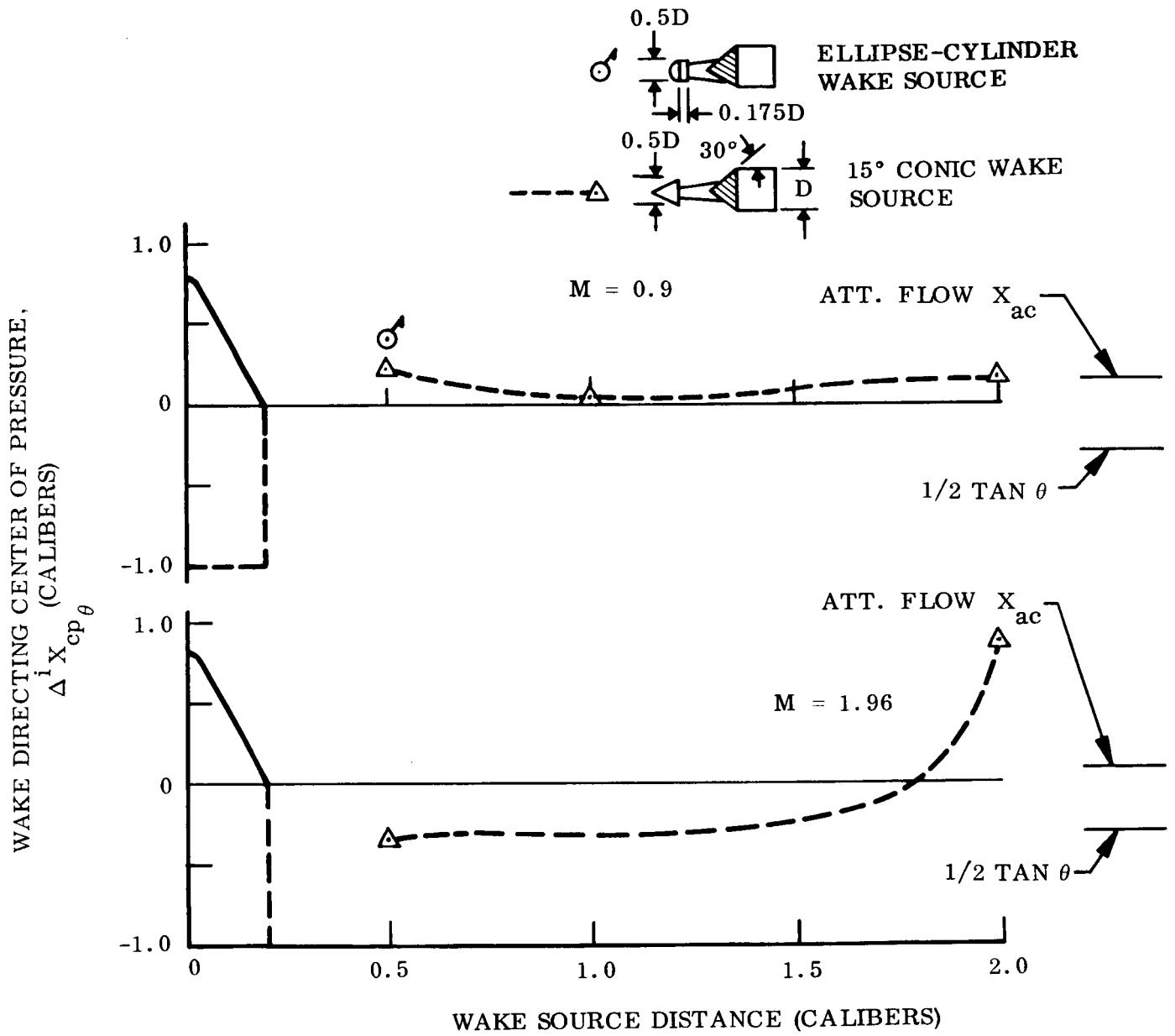


Fig. 21 Wake Directing Effects on the Conic Forebody Center of Pressure

CONCLUSION

Experimental data have been obtained on a wake submerged body which indicate the loads on the submerged body are dependent upon:

- 1) submerged body crossflow
- 2) relative lateral displacement of wake source and submerged body
- 3) wake source attitude

Furthermore, the rather unsophisticated technique of predicting the local loads from the submerged body separated to attached flow axial force ratio is valid for the Saturn-Apollo geometry. For greater wake source distances substantial upstream communication effects occur for each of the submerged body derivatives. Recognition of these upstream effects is of paramount importance to any computation of the vehicle dynamics from the static force characteristic since these loads could have profound dynamic effects. A method for extracting this upstream communication component from each of the experimentally obtained submerged body derivatives has been indicated.

REFERENCES

1. Lockheed Missiles and Space Company, "Report on Saturn I-Apollo Unsteady Aerodynamics", by Lars-Eric Ericsson and J. Peter Reding, LMSC/A650215, February 1964, (U).
2. Lockheed Missiles and Space Company, "Static Loads on the Saturn I-Apollo Launch Vehicle", by J. Peter Reding and Lars-Eric Ericsson, LMSC TM 53-40-143 (LMSC/803185), August 1963, (U).
3. Lockheed Missiles and Space Company, "Automatic Carpet Plotting", by D. M. Jecmen, LMSC/805634, (to be published).
4. Brown Engineering Company, Inc. "Basic Data Release of Investigation to Determine the Dependence of Afterbody Loads on Forebody Attitude for Tower Mounted Wake Sources", by William C. Pope, Jr., Brown Engineering TM AA-7-64-2, July 21, 1964, (U).
5. Brown Engineering Company, Inc. "Basic Data Release of Phase II of Investigation to Determine the Dependence of Afterbody Loads on Forebody Attitude for Tower Mounted Wake Sources", by William C. Pope, Jr. Brown Engineering TM AA-1-65-4, January 20, 1965.
6. AEDC, "Static and Dynamic Testing of Conical Trailing Decelerators for the Pershing Re-entry Vehicle", by Jack D. Coats, AEDC TN-60-188, October 1960, (U).
7. NASA, "Aerodynamic Characteristics of Towed Cones Used as Decelerators at Mach Numbers from 1.57 to 4.65", by Nickolai Charczenko and John T. Mc Shera, NASA TN D-994, December 1961.
8. NASA, "Aerodynamic Characteristics of Towed Spheres, Conical Rings, and Cones Used as Decelerators at Mach Numbers from 1.57 to 4.65", by Nickolai Charczenko, NASA TN D-1789, April 1963.

9. NACA, "Some Measurements in a Rectangular Cutout", by Anatol Roshko, NACA TN 3488, August 1955, (U).
10. Nicoll, Kenneth M., "A Study of Laminar Hypersonic Cavity Flows", AIAA Preprint No. 64-47, January 1964, (U).
11. Lockheed Missiles and Space Company, "Steady Loads on Spiked Blunt Bodies of Revolution", by Lars-Eric Ericsson, IMSC TM 53-40-121 (IMSC-A312114), November 1962, (C).
12. NACA, "Equations, Tables, and Charts for Compressible Flow", by Ames Research Staff, 1953, NACA Report 1135, (U).
13. NASA, "Aerodynamic Characteristics of Spherically Blunted Cones at Mach Numbers from 0.5 to 5.0", by Robert V. Owens, May 2, 1962, NASA Marshall Space Flight Center MTP-AERO-61-38.
14. NASA, "Effects of Nose Shape and Afterbody Flare on the Transonic Characteristics of a Low-Fineness Ratio Body of Revolution", by Stuart L. Treon, Roy M. Wakefield, and Earl D. Knechtel, March 1960, NASA TM X-164, (C).
15. NASA, "Flow Separation on Ellipsoidal-Nosed Cylinder Flare Models at Transonic Mach Numbers", by Joseph W. Cleary, NASA TM X-506, May 1961, (C).
16. IMSC, "Separated Flow Effects on the Static Stability of Cone-Cylinder-Flare Bodies", by J. Peter Reding, IMSC TM 53-40-119 (IMSC/802336), (C).

APPENDIX ANOMENCLATURE

A	Axial force, coefficient $C_A = A/(\rho U^2/2) S$
$C_p$	Pressure coefficient, $C_p = \frac{P - P_\infty}{q_\infty}$
D	Reference diameter (submerged body base diameter)
$l$	Longitudinal distance between wake source and submerged body normal force vector
M	Mach number
m	Pitching moment, coefficient $C_m = m/(\rho U^2/2) S D$
N	Normal force, coefficient $C_N = N/(\rho U^2/2) S$
p	Pressure
$\bar{p}$	Average pressure
q	Dynamic pressure, $q = \rho U^2/2$
S	Reference area, $\pi D^2/4$
V	Velocity
$x$	Longitudinal distance between wake source and tower base (tower length)
z	Vertical wake displacement

$\alpha$	Angle of attack
$\beta$	Angular translation of wake source
$\Delta, \delta$	Increment
$\xi_t$	Tower attitude
$\theta$	Wake source attitude relative to submerged body centerline
$\theta_t$	Wake source attitude relative to tower centerline
<u>Subscripts</u>	
a	Attached flow
b	Base
l	Leeward
s	Separated flow
T	Total
u	Uncorrected
v	Vertical perturbation velocity
w	Windward
$\infty$	Undisturbed flow
o	Conditions at $\alpha = 0$

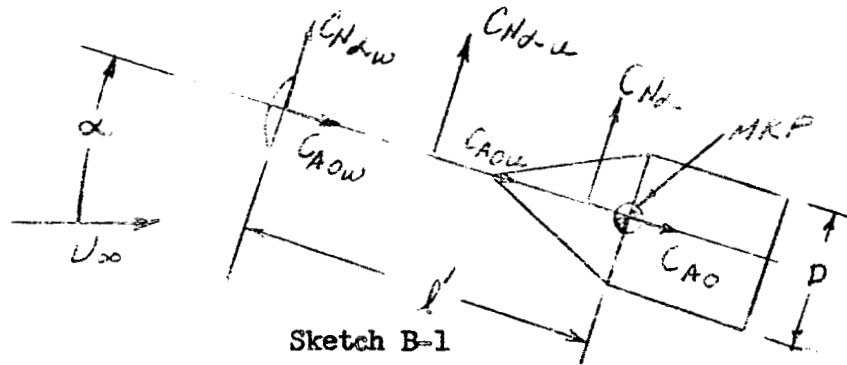
Superscripts

i	Denotes induced increment e.g., $\Delta^i C_N$ = induced increment in normal force coefficient
/	Upstream induced component

APPENDIX B

FINAL CORRECTIONS TO THE FORCE DERIVATIVES

The final step in the data reduction was to eliminate the wake source loads from the  $\alpha_u$ ,  $\theta_u$ , and  $\beta_u$  derivatives (the subscript u denotes data uncorrected for wake source loads). The wake source body axis loads were measured in the presence of the aft body. For the  $\alpha_u$  corrections one need only subtract the wake source loads since both wake source and submerged body load are in the same coordinate system as shown in Sketch B-1.



Thus

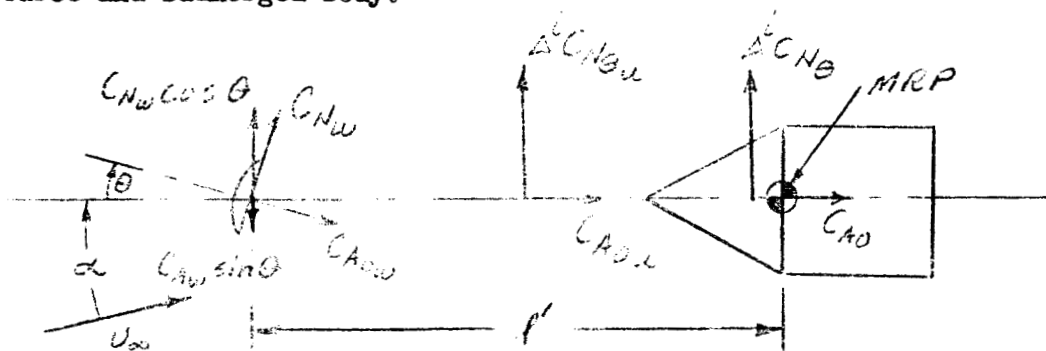
$$C_{N_x} = C_{N_{x,u}} - C_{N_{x,w}}$$

$$C_{A_0} = C_{A_{0,u}} - C_{A_{0,w}}$$

$$C_{M_x} = C_{M_{x,u}} - C_{N_{x,w}} \frac{l'}{D}$$

B-1

For the  $\theta_u$  corrections one must account for the difference in attitude between wake source and submerged body.



Sketch B-2

B-1



If

$$\Delta^i C_{N\theta} = \Delta^i C_{N\theta u} - \delta C_{N\theta}$$

$$\Delta^i C_{M\theta} = \Delta^i C_{M\theta u} - \delta C_{M\theta}$$

One may compute the correction terms  $\delta C_{N\theta}$  and  $\delta C_{M\theta}$  with the help of Sketch B-2,

and

$$\delta C_N = C_{Nw} \cos \theta - (C_{A0w} + \frac{\partial C_{A0w}}{\partial \theta}) \sin \theta$$

$$\delta C_M = \frac{r'}{D} C_{Nw} \cos \theta - \frac{r'}{D} (C_{A0w} + \frac{\partial C_{A0w}}{\partial \theta}) \sin \theta$$

differentiating the above for  $\theta=0$ ,  $\frac{\partial C_{A0w}}{\partial \theta} = 0$ ,  $\sin K\theta = 0$ ,  $\cos K\theta = 1$

yields

$$\delta C_{N\theta} = C_{N\theta w} - C_{A0w}$$

similarly

$$\delta C_{M\theta} = \frac{r'}{D} (C_{N\theta w} - C_{A0w})$$

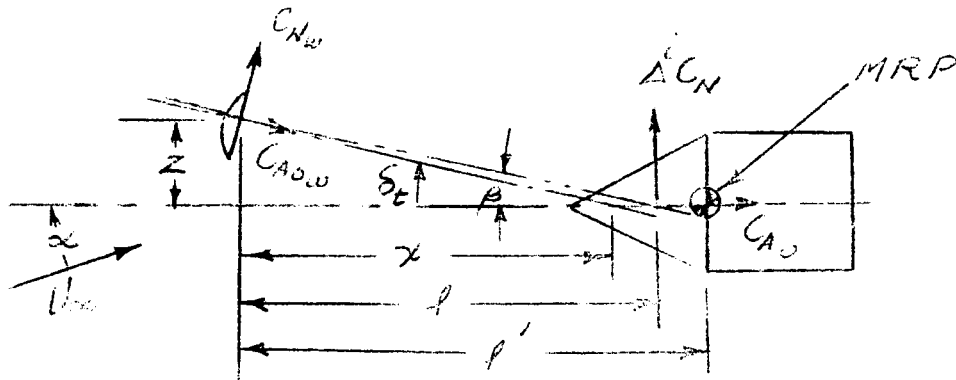
Therefore,

$$\Delta^i C_{N\theta} = \Delta^i C_{N\theta u} - (C_{N\theta w} - C_{A0w})$$

$$\Delta^i C_{M\theta} = \Delta^i C_{M\theta u} - \frac{r'}{D} (C_{N\theta w} - C_{A0w})$$

B-2

Finally the  $\delta_t$  derivatives were corrected for wake source loads and  $\theta$  effects.



Sketch B-3

From Sketch B-3 for small values of  $\delta t$

$$\begin{aligned} \beta &= \tan \beta = z/l \\ \delta t &= \tan \delta t = z/x \\ \delta t &= (l/x)\beta = K\beta \end{aligned}$$

and  $\delta t = \theta_t$

Therefore, transforming the wake source load into the submerged body axis system

$$\begin{aligned} \delta C_N &= C_{N_w} \cos \delta t - \left( C_{A_{0w}} + \frac{\partial C_{A_w}}{\partial \delta t} \delta t \right) \sin \delta t \\ &= C_{N_w} \cos K\beta - (C_{A_{0w}} + C_{A_{\delta t} \delta t}) \sin K\beta \end{aligned}$$

where  $\frac{\partial C_{A_w}}{\partial \delta t} = C_{A_{\delta t} \delta t}$

differentiating with respect to  $\beta$  for  $\beta = 0$ ,  $C_{A_{\delta t} \delta t} = 0$ ,  $\sin K\beta = 0$ ,  $\cos K\beta = 1$  gives,

$$\delta C_{N\beta} = K \frac{\partial C_{N_w}}{\partial \delta t} - K C_{A_{0w}} = K (C_{N_{\delta t}} - C_{A_{0w}}) \tag{B-3}$$

Likewise transforming the moment

$$\begin{aligned} \delta C_m &= \frac{l'}{D} \left[ C_{N_w} \cos \delta t - (C_{A_{0w}} + C_{A_{\delta t} \delta t}) \sin \delta t \right] \\ &\quad - \frac{z}{D} \left[ C_{N_w} \delta t + (C_{A_{0w}} + C_{A_{\delta t} \delta t}) \cos \delta t \right] \end{aligned}$$

substituting  $\delta t = K\beta$  and  $z = \frac{x}{D} \tan \beta \approx \frac{x}{D} \beta$  and differentiating with respect to  $\beta$  for  $\beta = 0$ ,  $C_{A_{\delta t} \delta t} = 0$ ,  $\sin K\beta = 0$ ,  $\cos K\beta = 1$  yields

$$\delta C_{m\beta} = \frac{K l'}{D} (C_{N_{\delta t}} - C_{A_{0w}}) + \frac{x}{D} C_{A_{0w}} \tag{B-4}$$

The incremental derivatives (Eq. B-3 and B-4) are applied to the  $\beta_u$  derivatives along with the  $\theta$  derivatives as follows;

$$\begin{aligned} \Delta^i C_{N\beta} &= \Delta^i C_{N\beta} - \Delta^i C_{N\theta} - \delta C_{N\beta} \\ \Delta^i C_{m\beta} &= \Delta^i C_{m\beta} - \Delta^i C_{m\theta} - \delta C_{m\beta} \end{aligned} \tag{B-5}$$

since  $\theta = \delta t$  then  $\frac{\theta}{\beta} = K$  and substituting Eq. B-3 for  $\delta C_{N\beta}$

$$\Delta^i C_{N\beta} = \Delta^i C_{N\beta} - K (\Delta^i C_{N\theta} + C_{N_{\delta t}} - C_{A_{0w}}) \tag{B-6}$$

Likewise the induced translational moment may be computed from Equations B-4 and B-5 as follows;

$$\Delta^i C_{m\beta} = \Delta^i C_{m\beta u} - K \left[ \Delta^i C_{m\theta} - \frac{l}{D} (C_{N_{\delta t}} - C_{A0w}) \right] - \frac{7}{D} C_{A0w} \quad B-7$$